https://doi.org/10.5194/egusphere-2026-3719
Preprint. Discussion started: 8 July 2026

Relative contributions of CO_2 and ice sheets on the Mid-Pleistocene Transition

Jeanne Millot-Weil[1], Paul Valdes[1], and Alexander Farnsworth[1]

[1]University of Bristol, United Kingdom

Correspondence: Jeanne Millot-Weil (xk22684@bristol.ac.uk)

Abstract. The Mid-Pleistocene Transition (MPT) represents one of the most prominent and debated climate reorganizations within the long-term cooling trend of the last 3.6 million years. Although the role of ice sheets, greenhouse gases and their combined effects have all been implicated, their individual contributions to the MPT remain unresolved.

Here, we assess their respective roles using a unique set of four series of fully coupled equilibrium palaeoclimate model simulations spanning the last 3.6 Ma at 4-ka intervals, constrained by realistic boundary conditions. These simulations differ in their prescribed insolation, greenhouse gases and ice sheet forcings where a realistic baseline time evolving scenario is analysed against a series where each forcing is kept static throughout to constrain their individual impact on the MPT.

First, we evaluate the performance of the four sets of simulations including the combination of the three changing forcings against geological data. We find that the model captures the main characteristics of temperature variations identified by geological records, such as the global cooling trend over the past 3.6 Ma, acceleration of cooling at the MPT, with amplification of the glacial-interglacial cycles along with a change of pace from a 40-ka to a 100-ka cyclicity. Then, we compare the four simulated timeseries to untangle the individual role of each forcing through time and show that greenhouse gases exert a direct and dominant role on both the long-term global cooling trend and the shift in glacial-interglacial cyclicity associated with the MPT. Ice sheets primarily modulate the amplitude of glacial-interglacial variability through their influence on sea-ice formation and ocean circulation.

1 Introduction

Over the last 3.6 million years (Ma), the geological record has shown a pronounced long-term global cooling trend of approximately 2.3 ^{o}C (Clark et al., 2024). This cooling is evident across multiple proxy archives, including stable oxygen ratios (δ^{18}O) from benthic foraminifera (Westerhold et al., 2020) (Ahn et al., 2017), Mg/Ca ratios (Rohling et al., 2014) and Alkenone derived Sea Surface Temperature (SST) records (Clark et al., 2024). However, this cooling trend is not simply linear, but punctuated by two transitions, i) the intensification of Northern hemisphere glaciation between 2.5 and 3 million years (≈2°C cooling (Sosdian and Rosenthal, 2009) (Clark et al., 2024) (Kleiven et al., 2002)) marking the end of the Pliocene (5.3 until 2.6 Ma), and ii) the change in glacial-interglacial alternation from a 41-ka to a 100-ka pace between 750 ka and 1,250 ka called the Mid-Pleistocene Transition (MPT) (1.3°C cooling (Sosdian and Rosenthal, 2009)) (Herbert, 2023) (Raymo and Nisancioglu, 2003) (Shackleton and Opdyke, 1977) (Pisias and Moore, 1981).

https://doi.org/10.5194/egusphere-2026-3719
Preprint. Discussion started: 8 July 2026

Glacial-interglacial cyclicity is a well-known characteristic of the Quaternary and Late Pliocene climate and arises due to changes in insolation received at the top of the atmosphere as a result of the changing position of the Earth relative to the Sun. These variations are governed by three orbital parameters: eccentricity (≈ 100 ka cycle), obliquity (≈ 40 ka cycle), and precession (≈ 20 ka cycle). However, changes in Earth's orbit alone cannot explain the shift in Global Mean Surface Temperature (GMST) recorded during the MPT (Herbert, 2023) (Clark et al., 2006), suggesting a major role is being played by internal feedbacks such as ice sheet extent/volume and greenhouse gases variations (Herbert, 2023) (Berends et al., 2021b). While various studies highlighted the importance of a growing ice sheet to explain the shift in the pace of the glacial-interglacial to a 100-ka cycle during the MPT (Raymo, 1997) (Clark and Pollard, 1998) (Berends et al., 2021b), others have implicated greenhouse gas forcing playing a dominant role in explaining changes in ice sheet volume and extent (Willeit et al., 2019) (Chalk et al., 2017) (Clark et al., 2006). However, because these forcings co-evolved in tandem (Herbert, 2023), their respective roles in driving the MPT still remain unresolved.

Our current understanding of past variations in global climate largely stems from geological proxies, but from such observations alone it is difficult to discern how changes in orbit and the long-term decline of CO_2 lead to this cyclic behaviour of the Earth system. Palaeoclimate models offer an avenue to unravel the relative impact of the three most important drivers of variations in Quaternary climate: i) orbital forcing, ii) greenhouse gas concentrations and iii) ice sheet volume and extent. Additionally, they enable exploration of regional climate responses which can behave differently compared to global trends, depending on their geographic location and proximity to Northern hemisphere ice sheets (Clark et al., 2006) (Herbert, 2023). However, running a transient climate model to cover orbital-scale variations is a challenge because of the high computational cost and time required. To address this issue, various strategies have been employed from the use of intermediate complexity models to the acceleration of orbital forcing techniques to compress "real-time" variability into shorter model integrations ((Timm and Timmermann, 2007) (Zeller et al., 2023) (Yun et al., 2023)). Another approach circumvents the time-dependent boundary conditions problem by running in parallel multiple simulations with prescribed insolation, ice sheet and greenhouse gases, that correspond to a particular date. This method is called "snapshot simulations" and has been developed using the full complexity model HadCM3B (Valdes et al., 2017) (Hopcroft and Valdes, 2021) to previously cover the last 800,000 years (Singarayer and Valdes, 2010) (Armstrong et al., 2023) (Armstrong et al., 2019).

In this study, we present an extended version of snapshot simulations that cover the last 3.6 Ma. Four unique sets of 919 simulations (spaced approximately every 4000 years) have been performed with different prescribed insolation, realistic ice sheet and greenhouse gas concentration evolutions, that are treated as four forcing sets for the model. First, All_forcings includes variations in insolation, greenhouse gases, and ice sheets (forcings timeseries are shown on Fig.1 (a), in black). Then, OrbGhg and OrbIce isolate the effects of greenhouse gases and ice sheets, respectively, by holding the other forcing constant at pre-industrial level. Finally, OrbOnly includes insolation variations only, with pre-industrial greenhouse gases and ice sheets fixed. Simulation sets characteristics are shown on Tab.1.

Since insolation, ice sheet and greenhouse gases are prescribed to the model, this study cannot investigate the impact of one forcing on another. Investigating the role of the stability of the ice sheet on the CO_2 decrease during the MPT and vice-versa is therefore out of the scope of this study. It would require fully coupled climate-ice-sheet-carbon-cycle models. Instead, these

https://doi.org/10.5194/egusphere-2026-3719
Preprint. Discussion started: 8 July 2026

four snapshots sets combined allow to isolate the individual role of credible ice sheet reconstructions, greenhouse gases and insolation on temperature changes during the last 3.6 Ma (Tab.1). We first take advantage of the recently published proxy-stack from (Clark et al., 2024) to evaluate the performance of HadCM3BB compared to geological data both on global and regional temperature variations. Then, we explore the individual impact of each forcing by comparing the temperature timeseries from each snapshot set.

2 Methods

2.1 Model Description - HadCM3BB

The simulations presented here are performed with a recently updated version of HadCM3, a variant of the Hadley Center unified model (Pope et al., 2000) (Gordon et al., 2000). HadCM3 is a coupled atmosphere-ocean-vegetation model. The specific version used for this work, HadCM3BB, is described in detail in (Valdes et al., 2017) and (Hopcroft et al., 2020). The atmosphere has a horizontal resolution of 2.5°x 3.75° and 19 vertical levels, and 1.25°x 1.25° in the ocean with 20 vertical levels with finer resolution near the surface. Despite its relatively coarse resolution and lower complexity compared to recent state-of-the-art CMIP6 models, HadCM3 has been shown to accurately simulate the modern climate system (sitting in the middle of the CMIP5 pack (Valdes et al., 2017)) as well as the Quaternary and Deep-time climate (Hopcroft and Valdes, 2021) (Hopcroft et al., 2020) (Steinig et al., 2024). Its climate sensitivity of 3.9 for a doubling relative to preindustrial CO_2 level falls within the CMIP5-PMIP3 and CMIP6-PMIP4 models, and corresponds to the CMIP6 average (3.9) (Zelinka et al., 2020) and is above the ensemble PMIP4 mean (3.2) (Kageyama et al., 2021). Its main advantage is its computational efficiency which permits long simulations, large ensemble and sensitivity studies. The model includes a land surface scheme MOSES2.1 (Essery et al., 2001) which simulates energy fluxes and physiological processes. Nine surface types are incorporated by MOSES2.1 and are simulated by the vegetation component Top-down Representation of Interactive Foliage and Flora Including Dynamics (TRIFFID) (Cox, 2001). No interactive greenhouse gases cycle or ice model are included in this study. They are given by the boundary conditions described below. Moreover, the model version used here has been updated to include paleoclimate-informed changes to atmospheric convection and dynamic vegetation as described in (Hopcroft and Valdes, 2021). This update allows the model to simulate more accurately the "Green Sahara" during the Holocene, as well as the abrupt transition to modern conditions subsequently, as a naturally occurring emergent property of the model without affecting its performance in simulating pre-industrial climates (Hopcroft and Valdes, 2021). This version of the model is one of the very few models that are able to correctly simulate the "Green Sahara". This study uses this paleo-conditioned model to investigate the causes of climate transitions through the last 3.6 Ma.

2.2 Boundary Conditions and Experimental Design

The simulations have been forced by orbital parameters variations based on (Laskar et al., 2004). The resulting insolation received at the top of the atmosphere timeseries is shown on Fig.1 (a) A).

https://doi.org/10.5194/egusphere-2026-3719
Preprint. Discussion started: 8 July 2026

Ice sheets are treated as a model boundary condition for each period based on the reconstruction from (De Boer et al., 2014), derived from inverse forward modelling approach using benthic δ^{18}O records and the 3D ice-sheet-shelf model ANICE. The global, Northern and Southern hemispheres ice volume evolutions are shown on Fig.1 (b) A) and exhibit the largest variations as a result of the Northern hemisphere glaciations. Land-sea distribution, topography, bathymetry, and ice sheet extent are also modified based on the ice sheet reconstruction. The sea-level evolution used in this study has previously been shown to be in reasonable agreement with other reconstructions derived from both geological reconstructions and modelling studies (Berends et al., 2021a). In particular, it is comparable to the reconstruction of (Willeit et al., 2019), which is based on transient simulations performed with CLIMBER-2 coupled to the ice-sheet model SICOPOLIS (Fig.1 (a) B)). Nonetheless, the sea-level variations in (Willeit et al., 2019) exhibit more intense glacials over the last 1000 ka than those of (De Boer et al., 2014), whereas both reconstructions show similar glacial–interglacial amplitudes prior to the Mid-Pleistocene Transition (MPT; 1250–750 ka). Consequently, the intensification of glacials across the MPT is more pronounced in (Willeit et al., 2019) than in (De Boer et al., 2014). This contrast is important to consider when interpreting the behaviour of a climate model under different ice sheet forcings, here, we will assess this impact through an analysis against (Yun et al., 2023) simulation (forced by (Willeit et al., 2019) boundary conditions) and our simulations (see parts 3.1 and 4).

Greenhouse gases concentrations (CO_2, CH_4 and N_2O) are prescribed from Vostok Ice Core record (Berger et al., 1998) (Loulergue et al., 2008) (Spahni et al., 2005), for the last 800 ka. Then, the greenhouse gases forcing has been adapted from the 3.6 Ma CO_2 timeseries reconstruction from (Berends et al., 2021a) which was based on inverse modelling from benthic δ^{18}O. This CO_2 timeseries has been modified by applying a stronger trend to reach the Pliocene CO_2 concentration level of 400 ppm as proposed by the model intercomparison project PlioMIP (Haywood et al., 2016). Moreover, we have deduced the CO_2 equivalent (CO_2_eq) values based on the relationship between CO_2 and CO_2 equivalent of the first 800 ka. The final CO_2_eq timeseries used to force each snapshot is shown in black on Fig.1 (a) C), along with the original (Berends et al., 2021a) and (Willeit et al., 2019) reconstructions and geological records. Good agreement is shown between (Berends et al., 2021a) and our adapted reconstructions for the last 1.5 Ma, after which the imposed trend becomes apparent. Indeed, while (Berends et al., 2021a)'s reconstruction shows a CO_2 concentration of 253 ppm at 2 Ma, in accordance with (Yan et al., 2019)'s value, the CO_2_eq we use reaches 294 ppm. Disagreement increase at the Pliocene where our CO_2_eq attains the PlioMIP value of 400 ppm while (Berends et al., 2021a)'s value is 328 ppm. Imposing our CO_2_eq trend to reach the values propose by PlioMIP ensures that the climate model can attain Pliocene temperatures, given its climate sensitivity (3.9).

These three (continental ice sheet volume and extent, greenhouse gases and orbital variations) boundary conditions have been included in each of the 919 snapshot experiments that span the last 3.6 Ma. For the first 24 ka before present (BP), these are set at 1 ka intervals then, from 24 ka until 3.6 Ma BP at 4 ka intervals. Each simulation has been run for at least 500 model years reaching a quasi-equilibrium state for the atmosphere and surface ocean. They were run in parallel, using initial conditions based on previous simulations covering the last 120 ka (Davies-Barnard et al., 2014), choosing the nearest equivalent sea level for each period. The last 100 years of each simulation were used to calculate the climate means. We call this initial snapshot simulations set All_forcings, as it includes the variations of all orbital scale parameters.

https://doi.org/10.5194/egusphere-2026-3719
Preprint. Discussion started: 8 July 2026

Three additional snapshot simulation sets have been created to explore the sensitivity to ice sheet, greenhouse gases and insolation changes. One of them includes time varying insolation and greenhouse gases but has a fixed pre-industrial ice sheet for every 919 snapshots, referred to here as OrbGhg. The second has time varying insolation and ice sheets but a constant pre-industrial CO_2_eq, called OrbIce. While the last, called OrbOnly, only includes insolation variations with both ice sheet and greenhouse gases fixed at pre-industrial state (see Tab.1).

In total, we performed more than 3600 simulations totalling more than 2 million model years.

Series	Ice sheet	Greenhouse gases	Orbital parameters
All_forcings	**Changing**	**Changing**	**Changing**
OrbGhg	Constant	**Changing**	**Changing**
OrbIce	**Changing**	Constant	**Changing**
OrbOnly	Constant	Constant	**Changing**

Table 1. Summary of Simulation Sets Characteristics

3 Results

3.1 Evaluating model results against geological data

Before examining the mechanisms driving these changes, it is necessary to evaluate the ability of the All_forcings experiment to reproduce the observed temperature evolution recorded in proxy-archives. To do so, we used the recently published 4.5 Ma global and regional temperature stack (Alkenone, Mg/Ca and Faunal records) of (Clark et al., 2024). In addition to comparisons with geological records, we also evaluate our results against previous modelling studies that employed a different approach to generate long-term variability. In particular, we draw on the 3 Ma CESM transient simulations presented in (Yun et al., 2023), which differs from our approach in both modelling methodology and boundary conditions. Their transient approach focused on accelerating the orbital year by a factor of five. Note that a different set of prescribed greenhouse gas concentrations and ice-sheet boundary conditions based on the reconstructions of (Willeit et al., 2019) were also used, shown in Fig.1 (a) B) & C) (purple). They did not include an estimate of the effects on non-CO_2 greenhouse gases, and Antarctica did not change throughout the whole time period.

To compare All_forcings with geological stacks and the simulation of (Yun et al., 2023), global, hemispheric and tropical temperatures are expressed as anomalies relative to their respective pre-industrial (0 ka) states. All model outputs and geological reconstructions are therefore consistent and comparable and presented as temperature changes relative to pre-industrial conditions. Timeseries comparisons are shown in Fig.2 for Global Mean Surface Temperature (ΔGMST) (a-left) (variable not available for (Yun et al., 2023)'s simulation), Global Mean Sea Surface Temperature (ΔGMSST) (a-right), Northern Hemisphere Mean Sea Surface Temperature (NH ΔSST) (b-left), Southern Hemisphere Mean Sea Surface Temperature (SH ΔSST) (b-right) and Tropical Mean Sea Surface Temperature (TROP ΔSST) (c-left).

https://doi.org/10.5194/egusphere-2026-3719
Preprint. Discussion started: 8 July 2026

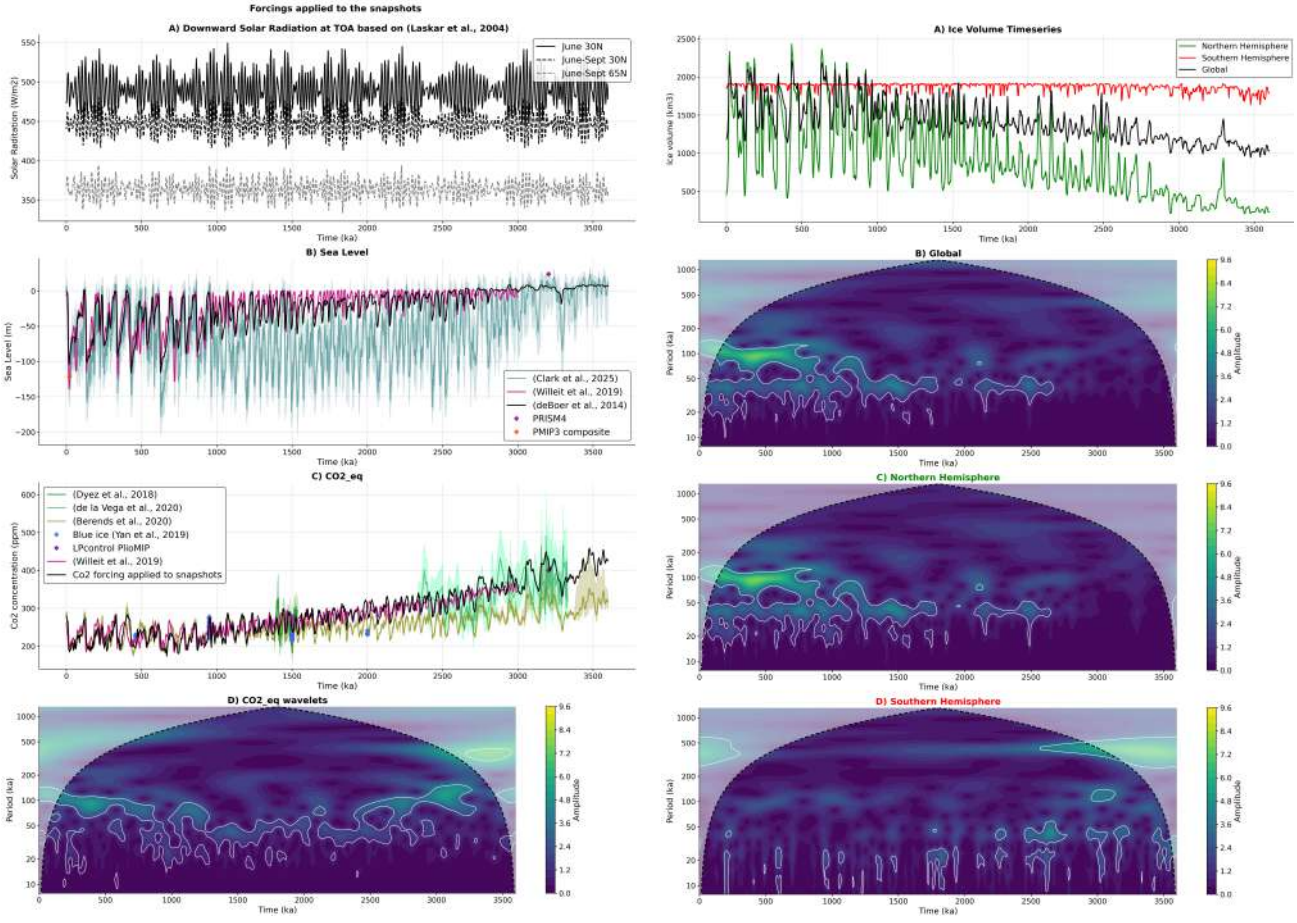

(a) (b)

Figure 1. Insolation, CO2 equivalent (CO2_eq) and ice sheet forcings applied to the simulations. (a) Boundary conditions applied to snapshots are in black: A) Insolation variations from (Laskar et al., 2004), B) Sea level from (De Boer et al., 2014) compared with (Clark et al., 2025a) and (Willeit et al., 2019) reconstructions, PRISM4 (Dowsett et al., 2016) and PMIP3 (Abe-Ouchi et al., 2015) estimations, C) CO_2 equivalent compared with (Berends et al., 2021a), (Willeit et al., 2019) reconstructions and geological data from (Yan et al., 2019), de la (De La Vega et al., 2020) and (Dyez et al., 2018) and with the CO_2 given to PlioMIP control runs (Haywood et al., 2024), D) Wavelet power spectrum of the CO_2 timeseries above (black). b) A) Global, Northern and Southern hemispheres ice volume evolution prescribed to the snapshots and their associated wavelet power spectra (B), C) and D) respectively).

Overall, Fig.2 shows that the All_forcings simulation successfully reproduces temperature variations derived from the geological data. It captures the key long term trends (Tab.2), and the changes in magnitude of the glacial-interglacial cycles as well as the transition at the MPT. In general, it also captures many of the longer term changes better than (Yun et al., 2023). But there are some small deficiencies in the All_forcings simulation which we highlight in the following paragraph and which

https://doi.org/10.5194/egusphere-2026-3719
Preprint. Discussion started: 8 July 2026

differ from (Yun et al., 2023)'s simulation. As ever when performing model-data comparisons, the causes of any mismatches may be the result of climate model deficiencies, poor knowledge of the changes in forcing, and imperfections in the proxy climate data. While the modelling approach and the model chosen differ from our reconstruction, the comparison with (Yun et al., 2023)'s temperature evolution can give some insights regarding the role of the forcings chosen. Nonetheless, it is often difficult to fully understand which combination of factors contribute to any model-data mismatch, and is often a function of the region and the proxy. A comprehensive regional and local analysis is beyond the scope of this study, and a more complete discussion will be the subject of forthcoming investigation.

3.1.1 Global Mean Surface Temperature (ΔGMST)

ΔGMST timeseries from the model and proxy-stacks (Fig.2 (a - left)) show a broadly similar global cooling trend over time, although the trend from the proxy-stack is overall steeper than the All_forcings simulations (s_stack = -2.3 °C/ka; s_All_36 = -1.5 °C/ka). To investigate when the model underestimates the cooling tendency relative to the proxy stack, we calculate trends over three distinct time slices: (i) before the MPT (3.6–1.25 Ma), (ii) during the MPT (1.25 Ma–750 ka), and (iii) after the MPT (750–0 ka). These intervals are characterised by glacial–interglacial cycles that differ in both periodicity and intensity. As such, rather than considering only the overall trends within each time slice, we focus on the trends of the glacial and interglacial peaks, defined as local minima and maxima of the timeseries (Tab.2). Before and after the MPT, the snapshots and proxy stack show comparable trends in both glacial and interglacial temperatures (s_stack$_{gl_preMPT}$ = 2.1 °C/ka, s_stack$_{igl_preMPT}$ = 1.6 °C/ka; s_All$_{gl_preMPT}$ = 1.6 °C/ka, s_All$_{igl_preMPT}$ = 1.5 °C/ka), although agreement is generally better for interglacial than for glacial trends (Fig. 2 (a, left); Tab. 2). This contrast becomes more pronounced during and after the MPT, when the All_forcings simulations underestimate the glacial cooling trend inferred from the ΔGMST of (Clark et al., 2024) (s_stack$_{gl_MPT}$ = 7.2 °C/ka, s_stack$_{igl_MPT}$ = 5.8 °C/ka; s_All$_{gl_MPT}$ = 3.7 °C/ka, s_All$_{igl_MPT}$ = 5.0 °C/ka; s_stack$_{gl_postMPT}$ = 0.8 °C/ka, s_stack$_{igl_postMPT}$ = -0.2 °C/ka; s_All$_{gl_postMPT}$ = -0.1 °C/ka, s_All$_{igl_postMPT}$ = -0.9 °C/ka) , while interglacial trends remain in better agreement. Despite these discrepancies, especially accentuated during the MPT, the modelled ΔGMST remains within the lower bound of the uncertainty range (yellow shade) reported by (Clark et al., 2024), and is also consistent with the PlioMIP results for the Pliocene (purple scatter, (Haywood et al., 2020)).

In addition to the long-term temperature trends, the All_forcings simulation set captures orbital-scale variability, although its amplitude differs from that of the proxy stacks. To quantify these differences, we compute the mean absolute deviation from the detrended time series ($\overline{abs\_dev}$; Tab.2) for the same three time slices defined above. Prior to the MPT, the All_forcings simulation overestimates the deviation from the mean relative to the stack of (Clark et al., 2024) ($\overline{abs\_dev}(stack\_preMPT)$ = 0.46 °C; $\overline{abs\_dev}(All\_preMPT)$ = 0.54 °C), whereas during and after the MPT the opposite behaviour is observed ($\overline{abs\_dev}(stack\_MPT)$ = 1.2 °C; $\overline{abs\_dev}(All\_MPT)$ = 0.8 °C; $\overline{abs\_dev}(stack\_postMPT)$ = 1.4 °C; $\overline{abs\_dev}(All\_postMPT)$ = 1.1 °C). Consequently, All_forcings does not reproduce the same increase in intensity of glacial–interglacial amplitude at the MPT as inferred from the proxy stack. This discrepancy can be attributed to the overestimation of glacial temperatures, consistent with the differences in glacial trends discussed above (Fig.2 (a) - see blue trends). A meaningful example of this difference in glacial intensity is the Last Glacial Maximum (LGM, 21 ka BP), for which the corresponding snapshot shows a

https://doi.org/10.5194/egusphere-2026-3719
Preprint. Discussion started: 8 July 2026

warmer GMST than both the proxy stack and its upper uncertainty bound (ΔGMST_model = -3.8 °C whereas ΔGMST_stack = -5.5 °C). When compared with other climate model outputs, specifically those from PMIP3/CMIP5, All_forcings remains warmer than the multi-model mean (ΔGMST_pmip = -4.4 °C) but still lies within the overall model spread (orange diamond and vertical line on Fig.2(a - left)). Note that the greenhouse gas, and orbital forcings are very similar to the PMIP3 standard for the LGM. However, the ice sheet is different and (Izumi et al., 2023) showed that alternative LGM ice sheets can alter global temperatures by more than 1.5 ^{o}C.

3.1.2 Global Mean Sea Surface Temperature (ΔGMSST)

The relationship between ΔGMST and ΔGMSST timeseries from (Clark et al., 2024)'s stack is close to the one obtained with All_forcings (Fig. 2 (d)). However, the differences identified in the ΔGMST time series are amplified when comparing the ΔGMSST reconstructions (Fig. 2 (a, right)). In particular, the ΔGMSST simulated by All_forcings does not reach sufficiently warm temperatures (between 3 and 3.6 Ma before present, $\Delta\text{GMST}_{stack}$ - $\Delta\text{GMST}_{All\_forcings}$ = 1.38 ^{o}C; $\Delta\text{GMSST}_{stack}$ - $\Delta\text{GMSST}_{All\_forcings}$ = 1.02 ^{o}C) during the Pliocene to fall within the uncertainty range reported by (Clark et al., 2024), nor within that inferred from the PRISM reconstructions, especially during glacial intervals (pink rectangle (McClymont et al., 2020)). Additionally, both glacial and interglacial temperature trends are weaker in our snapshots than in the ΔGMSST reconstruction of (Clark et al., 2024), particularly during the MPT (s_stack_{gl_MPT} = 4.3 °C/ka, s_stack_{igl_MPT} = 4.3 °C/ka; s_All_{gl_MPT} = 1.7 °C/ka, s_All_{igl_MPT} = 1.7 °C/ka), and are accompanied by an underestimation of glacial event amplitudes in the All_forcings simulation from the start of the MPT (≈ 1250 ka) ($\overline{abs\_dev}(stack\_MPT)$ = 0.6 °C; $\overline{abs\_dev}(All\_MPT)$ = 0.4 °C; $\overline{abs\_dev}(stack\_postMPT)$ = 0.8 °C; $\overline{abs\_dev}(All\_postMPT)$ = 0.5 °C). The LGM still provides a good illustration of the lower amplitude of glacial temperature of the model relative to geological data, with the ΔGMSST in the proxy stack being approximately twice as cold as in the model (ΔGMSST_model = -1.5 °C , ΔGMSST_stack = -3.0°C). Nevertheless, the snapshot LGM temperature is closer to the PMIP3 multi-model mean, and within the overall model spread (ΔGMSST_pmipmean = -1.7°C, orange diamond and vertical line).

Interestingly, the transient simulation of (Yun et al., 2023) shows better agreement with (Clark et al., 2024) in terms of glacial amplitudes during and after the MPT than either All_forcings or the PMIP3 LGM simulations (Fig.2 (a, left)). In contrast, ΔGMSST from (Yun et al., 2023) exhibits consistently lower values prior to the MPT than those obtained with All_forcings and, consequently, than those given by the (Clark et al., 2024) stack. The differences between the forcings used in our experiments and those employed by (Yun et al., 2023) can provide insight into the discrepancies observed between the respective ΔGMSST timeseries. Notably, the sea level evolutions implied by the ice sheet forcing from de (De Boer et al., 2014) used for our simulations and from (Willeit et al., 2019), used by (Yun et al., 2023), differ from one another (Fig.1 (a) B). Indeed, before the MPT, the sea level reconstruction from (Willeit et al., 2019) exhibits higher sea level than that of de (De Boer et al., 2014) ($\overline{sea\_level_{Willeit}}\_preMPT$ = -9.7 m; $\overline{sea\_level_{deBoer}}\_preMPT$ = -14.7 m), whereas after the MPT, both reconstructions show comparable levels ($\overline{sea\_level_{Willeit}}\_postMPT$ = -48.4 m; $\overline{sea\_level_{deBoer}}\_postMPT$ = -48.4 m), indicating a steeper MPT transition from (Willeit et al., 2019). Moreover, post_MPT glacials are generally more intense in (Willeit et al., 2019) than in (De Boer et al., 2014). For instance at the LGM, (Willeit et al., 2019) exhibits a sea level of 135.4

https://doi.org/10.5194/egusphere-2026-3719
Preprint. Discussion started: 8 July 2026

m below present for only 97.2 m below present for (De Boer et al., 2014) reconstruction, which is higher than the composite sea level of PMIP3 (121.5 m below present) (Abe-Ouchi et al., 2015). As such, the ice sheet evolution chosen to constrain the model is likely important to accurately represent the glacial temperature at the MPT and after. It should be noted that both (De Boer et al., 2014) and (Willeit et al., 2019) sea level reconstructions underestimate that of (Clark et al., 2024) during glacials and interglacials before the MPT and during glacial thereafter. On the other hand, greenhouse gas forcing by (Yun et al., 2023) (Willeit et al., 2019) and those used in this study are comparable (Fig.1 (a) C). Nonetheless, the CESM version used by (Yun et al., 2023) has a lower sensitivity for a doubling pre-industrial CO2 level than HadCM3 (2.4 and 3.9 respectively) which can, in part, explain the lower temperature observed in (Yun et al., 2023) than in All_forcings prior the MPT. While the forcings and sensitivity of the models are important for understanding their different behaviour (as pointed in (Clark et al., 2024)), both CESM and HadCM3 have inherent parametrisations and dynamics that can influence model responses.

3.1.3 Regional Sea Surface Temperatures (ΔNH_SST, ΔSH_SST and ΔTROP_SST)

Comparing SST signals for the Northern and Southern hemispheres (Fig.2 (b)) and for the Tropics (Fig.2 (c-left)) allows us to identify which region contributes the most to the discrepancies observed at global scale. In particular, when comparing to the geological reconstructions, All_forcings and (Yun et al., 2023) ΔGMSST simulations are amplified for the Southern hemisphere but reduced for the Northern hemisphere (Tab.2). Notably, the temperature discrepancy observed in the global timeseries during the late Pliocene appears to originate primarily from Southern hemisphere temperatures, as well as from the substantial differences in glacial temperatures from the MPT between All_forcings and the SST stack. This may reflect a combination of a lack of sensitivity from the models and a more accurate representation of Northern hemisphere ice-sheet changes compared to the Southern hemisphere, which varies substantially less than the Northern hemisphere in our simulations (Fig. 1b, A)) and is held constant in the transient simulation of (Yun et al., 2023). However, it should also be noted that the Southern hemisphere reconstruction from (Clark et al., 2024) have larger uncertainties compared to the Northern hemisphere stack due to the limited availability of proxy records in that region (Fig.A1). This uneven proxy coverage may introduce a Northern hemisphere bias in (Clark et al., 2024) global reconstructions, potentially contributing to the stronger model–data agreement in that hemisphere.

Comparing SST signals in the tropics (Fig.2 (c)) provides a useful constraint on the greenhouse gas forcing in our simulations as this region is primarily sensitive to CO_2 rather than ice sheet variability (Broccoli, 2000) (Ford and Ravelo, 2019). Moreover, geological records from this region, being distant from polar ice sheets, are often used to infer past CO_2 variations (De Garidel-Thoron et al., 2005) (Dyez and Ravelo, 2013).

Accordingly, the glacial-interglacial amplitude after the MPT is significantly smaller in (Clark et al., 2024)'s tropical SST reconstruction than for the hemispheric ones ($\overline{abs\_dev}$ = 0.56 °C and $\overline{abs\_dev}$ = 0.81 °C respectively; Tab.2). All_forcings does not reproduce a such large post MPT difference in glacial-interglacial intensity between hemispheric and tropical SSTs ($\overline{abs\_dev}(NH\Delta SST)$ = 0.47 °C, $\overline{abs\_dev}(SH\Delta SST)$ = 0.52 °C and $\overline{abs\_dev}(TROP\Delta SST)$ = 0.48 °C respectively; Tab.2). Consequently, the discrepancy in glacial-interglacial amplitude of variability between the model and the geological stack observed after the MPT at global and hemispheric scales is reduced, leading to improved model-data agreement. At this

https://doi.org/10.5194/egusphere-2026-3719
Preprint. Discussion started: 8 July 2026

time slice, the CO_2_eq variations applied to the snapshots comes from the Vostok Ice Core (Berger et al., 1998), (Loulergue et al., 2008), (Spahni et al., 2005) and are subject to much lower uncertainty than the rest of the 3.6 Ma record. This suggests that the discrepancies observed in TROPΔSST between All_forcings and the geological stack post MPT likely reflect an insufficient model sensitivity, which in turn can explain why prior MPT, the tropical SST from the model stays in the cooler uncertainty range of (Clark et al., 2024)'s reconstruction. TROPΔSST from (Yun et al., 2023)'s transient simulation, conducted with a less sensitive model to CO_2 than HadCM3, supports this interpretation as it remains cooler than All_forcings over the entire time slice.

Nevertheless, the post MPT greater contrast in glacial–interglacial intensity between hemispheric and tropical SSTs in (Clark et al., 2024)'s stacks, compared to All_forcings, raises questions about ice sheet sensitivity in both geological reconstructions and the model. On the one hand, the underestimation of the glacial-interglacial amplitude after the MPT in the model for both hemispheric SSTs suggests insufficient sensitivity to the prescribed ice sheet forcing. On the other hand, the improved agreement between model and proxy records in the tropics during the same period, and in the Northern hemisphere during the Early to Mid-Pleistocene (Fig.2 (b-left)), when Northern hemisphere ice sheet volume is reduced (Fig.1 (b) A)), may indicate that the geological records used to construct the stacks of (Clark et al., 2024) are overly sensitive to ice sheet variations, particularly those from Greenland, where many records used for the stack are concentrated (Fig.A1). The better agreement found between geological and model ΔGMST timeseries (Fig.2 (a-left)) than between SSTs is another indication of a potential lack of open ocean records used to build the geological SST reconstructions.

Overall, All_forcings shows the principal characteristics exhibited in (Clark et al., 2024) geological stacks over the past 3.6 Ma, e.g., long term global cooling trend with intensification during the MPT and increase in amplitude of the ice age cycles after the MPT. These features are more muted in the model than in the geological reconstructions, suggesting either a lack of sensitivity from the model (and associated forcings, notably the ice sheet) and/or spatiotemporal bias in the proxy-stack, in particular undersampling of higher southern latitudes and open ocean records.

We now use the model simulations to analyse the mechanisms driving temperature variations over the past 3.6 Ma.

https://doi.org/10.5194/egusphere-2026-3719
Preprint. Discussion started: 8 July 2026

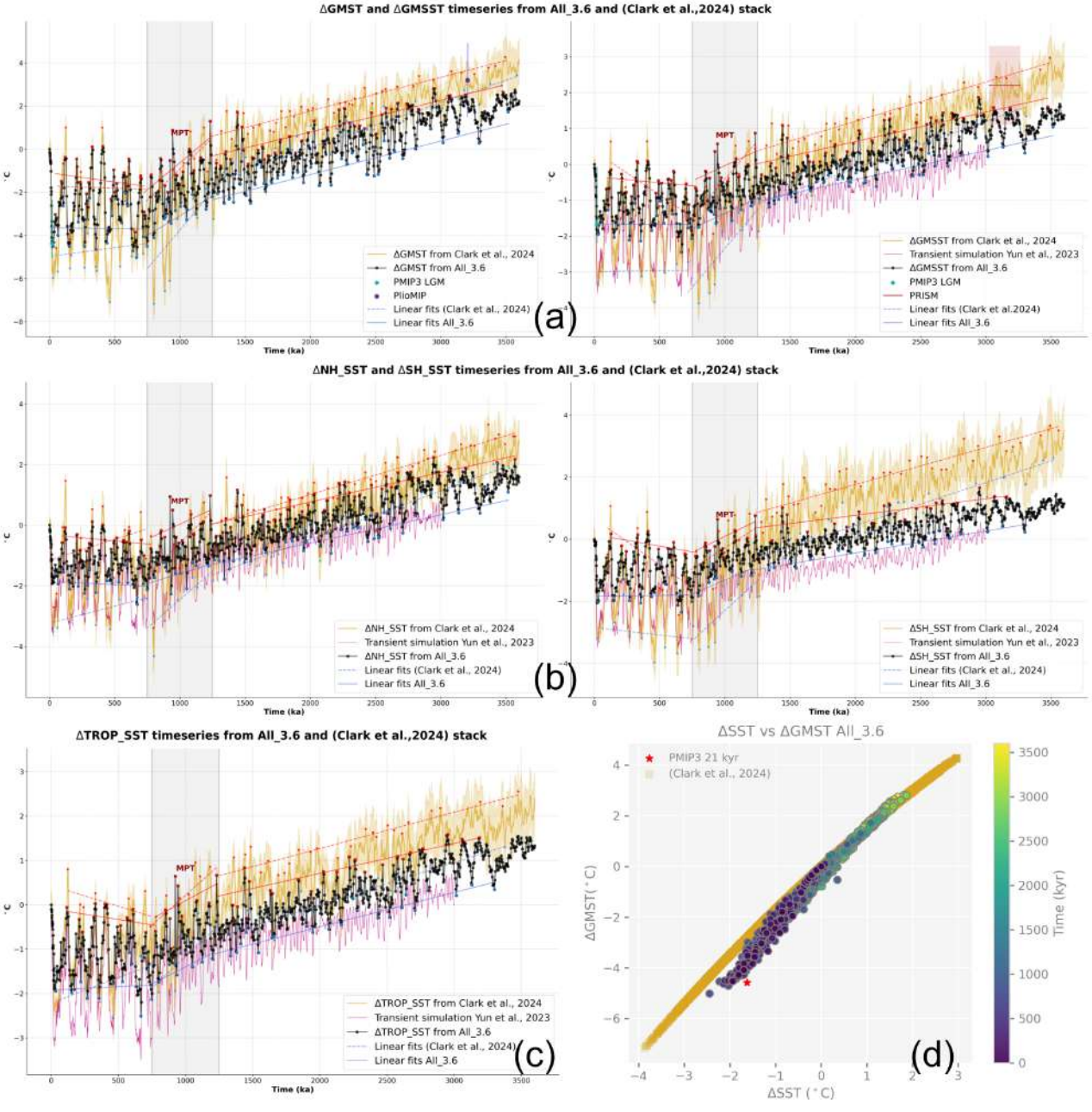

Figure 2. Temperature anomalies relative to pre-industrial conditions from All_forcings simulations, geological reconstructions, and transient simulations. Black dots are equilibrium simulations, yellow curves the geological stacks of (Clark et al., 2024), and purple curves the transient simulation of (Yun et al., 2023). (a) Global means surface and sea surface temperatures (ΔGMST and ΔGMSST). (b) Northern and Southern sea surface temperatures ΔNH_SST and ΔSH_SST). (c) Tropical sea surface temperature (ΔTROP_SST). Red and blue symbols indicate interglacial and glacial states; triangles correspond to All_forcings simulations and stars Clark et al. (2024) stacks. Solid and dashed lines show linear trends for simulations and reconstructions, respectively. Trends are shown separately for glacials and interglacials over the pre-MPT (3.6–1.25 Ma), MPT (1.25–0.75 Ma), and post-MPT (0.75–0 Ma) intervals. (d) Relationship between ΔGMST and ΔGMSST.

https://doi.org/10.5194/egusphere-2026-3719
Preprint. Discussion started: 8 July 2026

Reconstruction	Variable	Trends & $\overline{abs\_dev}$	3.6 Ma – 1250 ka	1250 – 750 ka	750 ka – 0
All_forcings/ Clark et al., 2024	ΔGMST	Gl slope	**1.555/** 2.079	**3.667/** 7.167	**-0.063/** 0.809
		IGl slope	**1.471/** 1.555	**5.011/** 5.789	**-0.855/** -0.216
		$\overline{abs\_dev}$	**0.54/** 0.46	**0.80/** 1.16	**1.10/** 1.44
	ΔGMSST	Gl slope	**0.807/** 1.309	**1.718/** 4.338	**-0.023/** 0.054
		IGl slope	**0.822/** 1.094	**1.691/** 4.289	**-0.339/** -2.452
		$\overline{abs\_dev}$	**0.30/** 0.30	**0.41/** 0.65	**0.53/** 0.79
	NH ΔSST	Gl slope	**0.935/** 1.587	**1.311/** 3.731	**-0.221/** 1.121
		IGl slope	**0.970/** 1.295	**1.978/** 4.260	**-0.404/** 1.376
		$\overline{abs\_dev}$	**0.36/** 0.38	**0.42/** 0.65	**0.47/** 0.81
	SH ΔSST	Gl slope	**0.704/** 1.389	**1.807/** 3.889	**0.059/** -0.481
		IGl slope	**0.533/** 1.198	**2.071/** 2.716	**-0.742/** -2.979
		$\overline{abs\_dev}$	**0.24/** 0.36	**0.32/** 0.72	**0.52/** 0.81
	TROP ΔSST	Gl slope	**0.776/** 0.958	**1.540/** 2.839	**0.152/** 1.147
		IGl slope	**0.676/** 0.819	**1.635/** 2.697	**-0.479/** -0.934
		$\overline{abs\_dev}$	**0.24/** 0.27	**0.35/** 0.47	**0.48/** 0.56

Table 2. Linear temperature trends for glacial (Gl) and interglacial (IGl) peaks (°C ka^{-1}), and **mean absolute deviation from the mean** (°C; $\overline{abs\_deviation} = |TS_{detrend} - \overline{TS\_detrend}|$) **for All_forcings (bold) and (Clark et al., 2024) geological stack**. Values are shown for 3.6–1.25 Ma (prior to MPT), 1.25–0.75 Ma (during the MPT) and 0.75–0 Ma (after the MPT).

3.2 Individual impact of insolation, ice sheet and greenhouse gases variations

This section aims to highlight the individual role of insolation, ice sheet and greenhouse gas forcings shown in Fig.1 on the simulated temperature variations over the last 3.6 Ma. Such sensitivity modelling studies have previously been carried out but have predominantly focused on individual time slices to identify the impact of specific forcings. However, when looking at a large spectrum of variability such as over the last 3.6 Ma and the mechanisms driving this variability, a different approach is required. By running the same series of simulations, but instead keeping one of the forcings static (at pre-industrial values), we can isolate the individual impact (amplitude (intensity) and pace) of that forcing on temperature.

To this end, we compare All_forcings set to three other comparable snapshots series: i) OrbGhg which includes the same varying insolation and greenhouse gases used in All_forcings but constant pre-industrial ice sheet, ii) OrbIce, including varying insolation and ice sheet but constant pre-industrial greenhouse gases concentration, and iii) OrbOnly that includes varying insolation only, ice sheet and greenhouse gases being set at pre-industrial levels for the entire 3.6 Ma. As for the evaluation of the model's performance, we study the variations of surface and sea surface temperature compared to pre-industrial values at global scale, over the Northern and the Southern hemispheres and over the Tropics (Fig.3, 4, 5 and 6 respectively). We focus in particular on the impact of each forcing on the key characteristics of the temperature time series identified above:

https://doi.org/10.5194/egusphere-2026-3719
Preprint. Discussion started: 8 July 2026

long-term global cooling trends, the intensification of glacial–interglacial amplitudes across the MPT, and the transition from predominantly 40-ka paced to 100-ka paced glacial–interglacial cycles.

3.2.1 Individual forcing impacts on cooling trends

The long-term cooling trends identified in both the geological stacks and the All_forcings simulations are absent from the OrbOnly temperature time series (Fig.3, 4, 5 and 6, yellow), in which temperature oscillates around a constant mean throughout the time slice. In contrast, both OrbGhg and OrbIce exhibit cooling trends (red and blue lines respectively on Fig.3, 4, 5 and 6), but weaker than that simulated by All_forcings (Fig.7 (a) & Tab.A2). This indicates that variations in greenhouse gases and ice sheets act in combination to reproduce the total cooling tendency found in All_forcings.

However, their contributions are not equivalent. Notably, OrbGhg are close to those found in All_forcings whereas OrbIce exhibits significantly weaker slopes (ΔGMST tendency is reproduced at 72% by OrbGhg and at 36% by OrbIce, and at 87% and 28% respectively for ΔGMSST tendency (Fig.7 (a) & Tab. A2), indicating a primary role played by greenhouse gas variations. This difference can be explained by the fact that only OrbGhg reproduces the Pliocene temperatures simulated in All_forcings. In contrast, when Northern ice-sheet cover is reduced, such as at the late Pliocene (Fig.1 (b) A))), OrbIce and OrbOnly are driven, or impacted by similar forcings (e.g.insolation), resulting in comparable temperature signals that are closer to pre-industrial values than the late Pliocene ones. Nonetheless, even though greenhouse gases play a major role in explaining the global cooling trend, their relative contributions vary between regions and between air and sea surface temperatures, with ice-sheet variations compensating for these differences.

In particular, at global and hemispheric scales, ice-sheet variations exert a stronger influence on surface air temperature trends than on sea surface temperature trends over the full 3.6 Ma, as well as over the shorter intervals defined above corresponding to the periods before, during, and after the MPT (Fig.3, 4, 5; right and left plots respectively, Fig.7 (a) and Tab.A2). This could partly be explained by the fact that surface air temperature averages are calculated over the entire domain considered (global, North hemisphere or South hemisphere) whereas SST is averaged only over ocean points, and excluding land ice covered areas (see Fig.A2 for land and sea ice covered areas). As a result, SST timeseries are less influenced by high-latitude regions, particularly during periods of large ice sheets. Nonetheless, computing the average air surface temperature by excluding the ice sheet areas (not shown) shows that this artefact impacts mainly the NH ΔST cooling trends, as the Northern hemisphere ice sheet is the one showing the major variations (Fig.1 (b) A)). Besides, none of the surface air temperature time series that exclude ice sheet covered areas fully reproduce the signals observed in the SST time series, revealing different response of the atmospheric and SST to the ice sheet forcing at global and hemispheric scales. However, this contrast in atmospheric and SST behaviour is not observed in the tropical timeseries (Fig.6, Fig.7 (a) and Tab.A2), suggesting that the particular influence of ice sheet cover on atmospheric temperatures is primarily restricted to high latitudes. Furthermore, OrbGhg closely reproduces the tropical temperature variability of All_forcings almost identically, whereas OrbIce stays close to the OrbOnly timeseries (Fig.6), confirming the dominant role of CO_2_eq and the limited influence of ice sheet variability on tropical surface temperatures.

https://doi.org/10.5194/egusphere-2026-3719
Preprint. Discussion started: 8 July 2026

With respect to the relative contributions of the different forcings on temperature trends across the three intervals, we find, as expected, that the contribution of greenhouse gases to temperature trends is greater during the pre-MPT interval than during the post-MPT interval, whereas the opposite pattern characterizes ice-sheet forcing (Fig.7 (a)). This reflects the tendencies in the forcings applied to the snapshots (Fig.1): during the pre-MPT interval, greenhouse gas concentrations decrease more rapidly than ice sheets grow, whereas after the MPT, ice sheet variations show greater amplitude of variations than the greenhouse gases. Interestingly, during the MPT, the trend slopes in both OrbGhg and OrbIce are generally closer to those observed in All_forcings than in the other intervals. While the intensification of glaciation during this time slice (Fig.1 (a) B) & (b) A)) accounts for the greater contribution of the ice sheet, no substantial change in the CO_2_eq trend is observed compared with the pre-MPT interval (Fig.1 (a) C)). In addition, the NHΔSST in OrbGhg exhibits a steeper cooling trend than in All_forcings. This highlights the role of an enhanced Northern hemisphere ice sheets found in OrbGhg compared to All_forcings during this time period. As highlighted in previous work (Tzedakis et al., 2017) (Berends et al., 2021b) (Chalk et al., 2017), to shape the MPT, the ice sheet needs to reach a threshold of steadiness to escape a glacial period. In All_forcings, the ice sheet gradually grows during the MPT, reaching volumes comparable to the later glacial–interglacial cycles, whereas in OrbGhg, a steady ice sheet is already present at the start of the MPT. This leads to a steep cooling trend, particularly in the Northern hemisphere, where ice-sheet changes are most pronounced (Fig.1 (b) A)).

The non-linear response of the climate system is also indicated by the changes in how the combined trends from OrbGhg and OrbIce compare with those from All_forcings over time (Fig.7 (a)). The sum of the trends from OrbGhg and OrbIce approximately matches those from All_forcings prior to the MPT, suggesting a linear climate response to both greenhouse gases and ice-sheet forcing. Conversely, this sum exceeds the slopes from All_forcings during the MPT and falls to approximately 10% below afterward (Fig.7 (a) & Tab.A2), suggesting a changed response of the temperatures to both forcings.

Overall, the global cooling trend observed in All_forcings is primarily driven by variations in greenhouse gas concentrations, although changes in ice sheet extent also play a role at mid to high latitudes, notably to explain the intensity of cooling during the MPT.

3.2.2 Individual forcings impacts on glacial-interglacial amplitudes

As observed for the trends, neither OrbGhg nor OrbIce fully reproduces the mean absolute deviation from the detrended temperature timeseries simulated in All_forcings across the different time slices (Fig.7 (b) & Tab.A1), highlighting the combined influence of ice-sheet and greenhouse gas variations in shaping the amplitude of glacial–interglacial cycles. Moreover, summing the mean absolute deviations obtained from OrbGhg, OrbIce and OrbOnly exceeds the values obtained for All_forcings (Fig.7 (b)), marking the non-linear response of glacial-interglacial temperatures to both forcings.

In contrast to the trends, OrbOnly (Fig. 3, 4, 5, 6, yellow) exhibits glacial–interglacial variability, that is directly driven by insolation changes at the top of the atmosphere. However, the extent to which it reproduces the amplitude of variability of All_forcings differs across time slices and regions. Prior to the MPT, insolations relative impact is the highest, and decreases as the ice sheet grows (Fig.7 (b)). Additionally, OrbOnly reproduces in higher rate the amplitude of variability of All_forcings

https://doi.org/10.5194/egusphere-2026-3719
Preprint. Discussion started: 8 July 2026

over the Tropics and the Northern hemisphere than over the Southern hemisphere (Fig.7 (b) & Tab.A1), which highlights where the insolation variations are the largest.

Ice sheet variability contributes more strongly to the amplitude of variability than to the temperature trends. For example, over the full 3.6 Ma, OrbIce reproduces 60% of the mean absolute deviation from the detrended ΔGMST time series of All_forcings, compared with only 35% for the trend (Fig.3, Tab.A1). The influence of ice-sheet variations on the amplitude of glacial–interglacial cycles is most pronounced for atmospheric surface temperature over the Northern hemisphere (Fig.(4); $\overline{abs\_dev}(OrbIce_{NH\Delta ST})$ reproduces 65% of All_forcings ; $\overline{abs\_dev}(OrbIce_{SH\Delta ST})$ and $\overline{abs\_dev}(OrbIce_{TROP\Delta ST})$ reproduces 55% of All_forcings), where ice sheet variations prescribed to the model are the largest (Fig.1 (b) A)). Conversely, greenhouse gases variations contribute relatively less strongly to the intensity of the glacial-interglacial cycles than to the temperature trends. Nonetheless, their impact is still major and the amplitude of variability in OrbGhg is close to what is obtained for OrbIce ($\overline{abs\_dev}(OrbGhg_{\Delta GMST})$ = 60% of All_forcings). Notably, the influence of greenhouse gases on glacial–interglacial amplitude is particularly pronounced in the Tropics across all time slices, and in Northern hemisphere SSTs as ice sheet and sea ice cover expand and increasingly mask the ocean surface from the MPT (Fig.7(b), Tab.A1, Fig.A2). This emphasizes the predominant impact of greenhouse gases in the Tropics and over the sea, while ice sheet variations mainly influences atmospheric surface temperatures at high latitudes, as observed for the trends.

In addition, as ice sheets expand from pre MPT to post MPT, the mean absolute deviations in OrbIce reproduce those of the All_forcings temperature time series less closely, while the opposite behaviour is observed for OrbGhg (Fig.7 (b) & Tab.A1), despite the amplitude of variability of both prescribed ice sheet and CO_2_eq increases over time (Fig.1). This suggests that CO2 variability alone can drive important glacial-interglacial surface temperature variations even under constant ice sheet conditions, whereas the dampening effect of fixed CO_2_eq is too strong for ice sheet variability alone to generate comparable variability.

Overall, while greenhouse gases are still a dominant contributor, these results highlight the important influence of ice sheet variations to explain the amplitude of glacial-interglacial cycles, as inferred from the comparison between (Yun et al., 2023) simulation and All_forcings set. This is particularly the case over high Northern hemisphere latitudes where the variations of glacial-interglacial temperatures are the highest, whereas over the Southern hemisphere the ice sheet variability is more modest, or over the Tropics which are remote from polar ice sheets, the relative influence of greenhouse gases is higher.

https://doi.org/10.5194/egusphere-2026-3719
Preprint. Discussion started: 8 July 2026

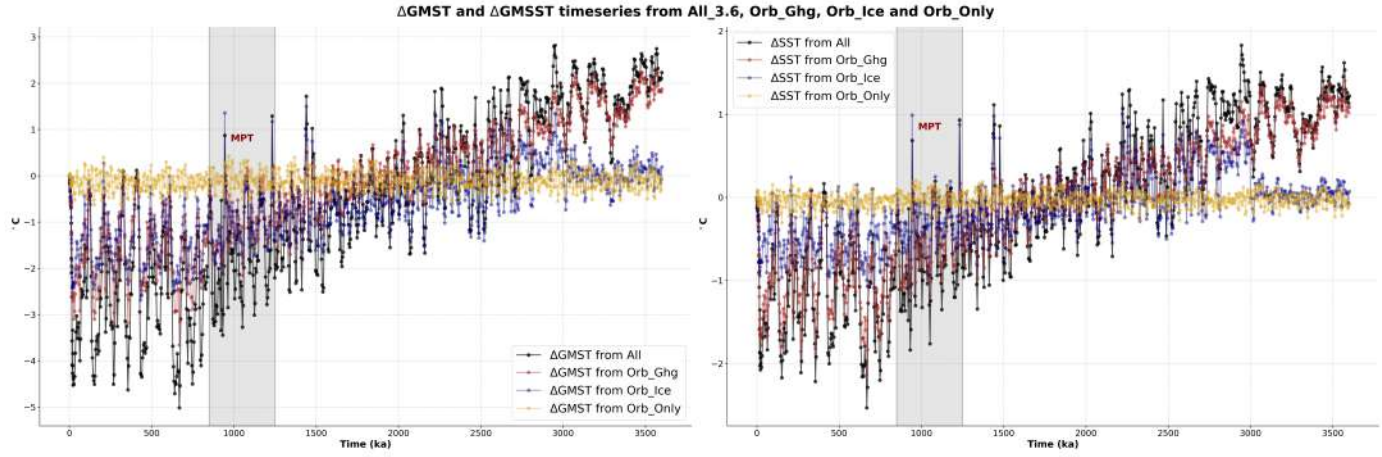

Figure 3. Global surface air temperature (ΔGMST) and global sea surface temperature (ΔGMSST) time series compared to pre-industrial for All_forcings (black), OrbGhg (red), OrbIce (blue), and OrbOnly (yellow).

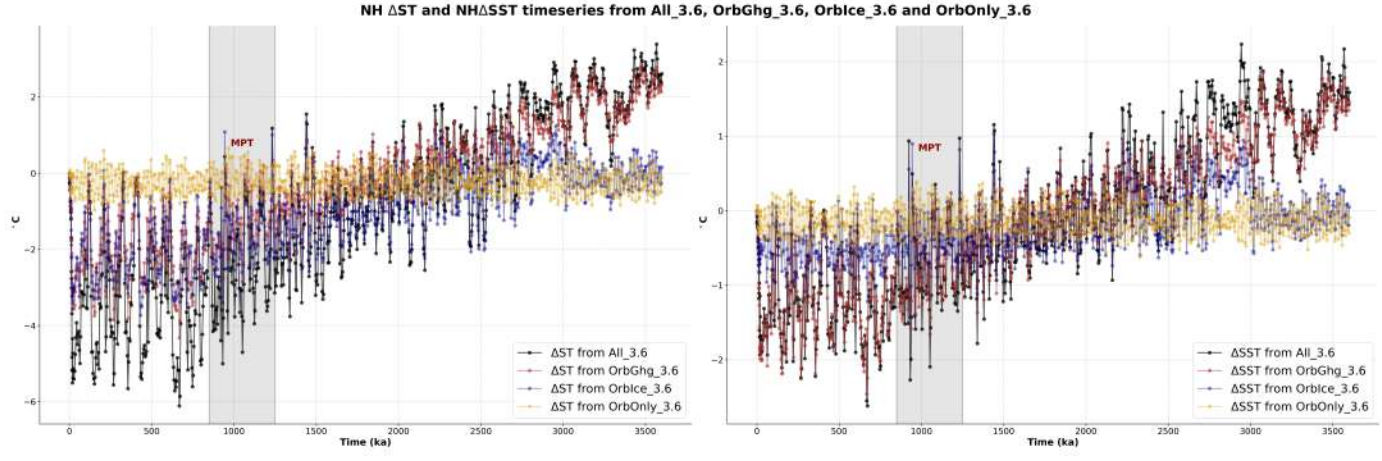

Figure 4. Northern surface air temperature (NHΔST) and northern sea surface temperature (NHΔSST) time series compared to pre-industrial for All_forcings (black), OrbGhg (red), OrbIce (blue), and OrbOnly (yellow).

https://doi.org/10.5194/egusphere-2026-3719
Preprint. Discussion started: 8 July 2026

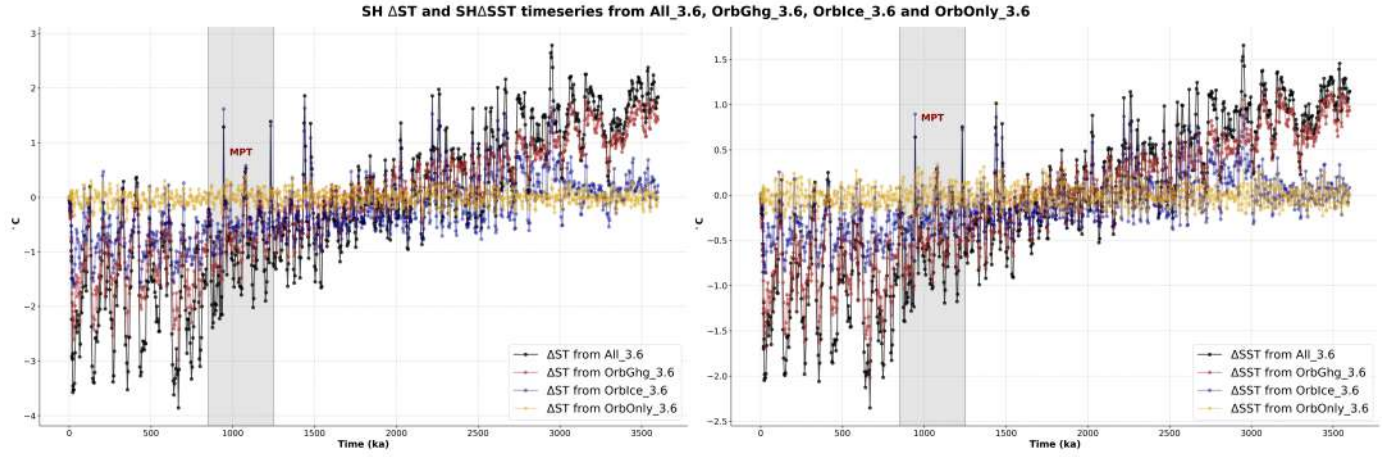

Figure 5. Southern surface air temperature (SHΔST) and southern sea surface temperature (SHΔSST) time series compared to pre-industrial for All_forcings (black), OrbGhg (red), OrbIce (blue), and OrbOnly (yellow).

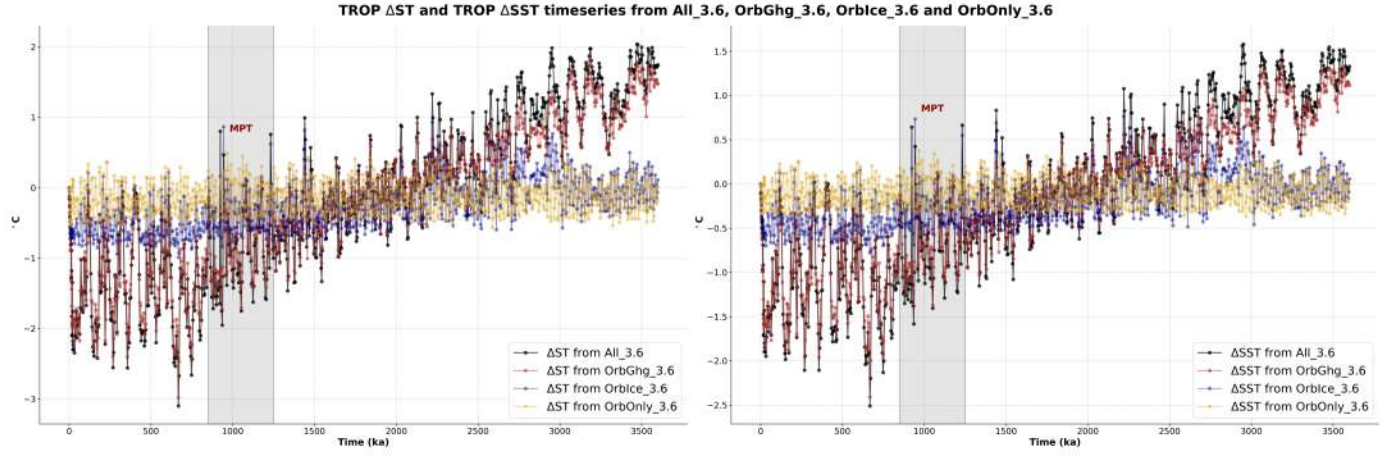

Figure 6. Tropical surface air temperature (TROPΔST) and tropical sea surface temperature (TROPΔSST) time series compared to pre-industrial for All_forcings (black), OrbGhg (red), OrbIce (blue), and OrbOnly (yellow).

https://doi.org/10.5194/egusphere-2026-3719
Preprint. Discussion started: 8 July 2026

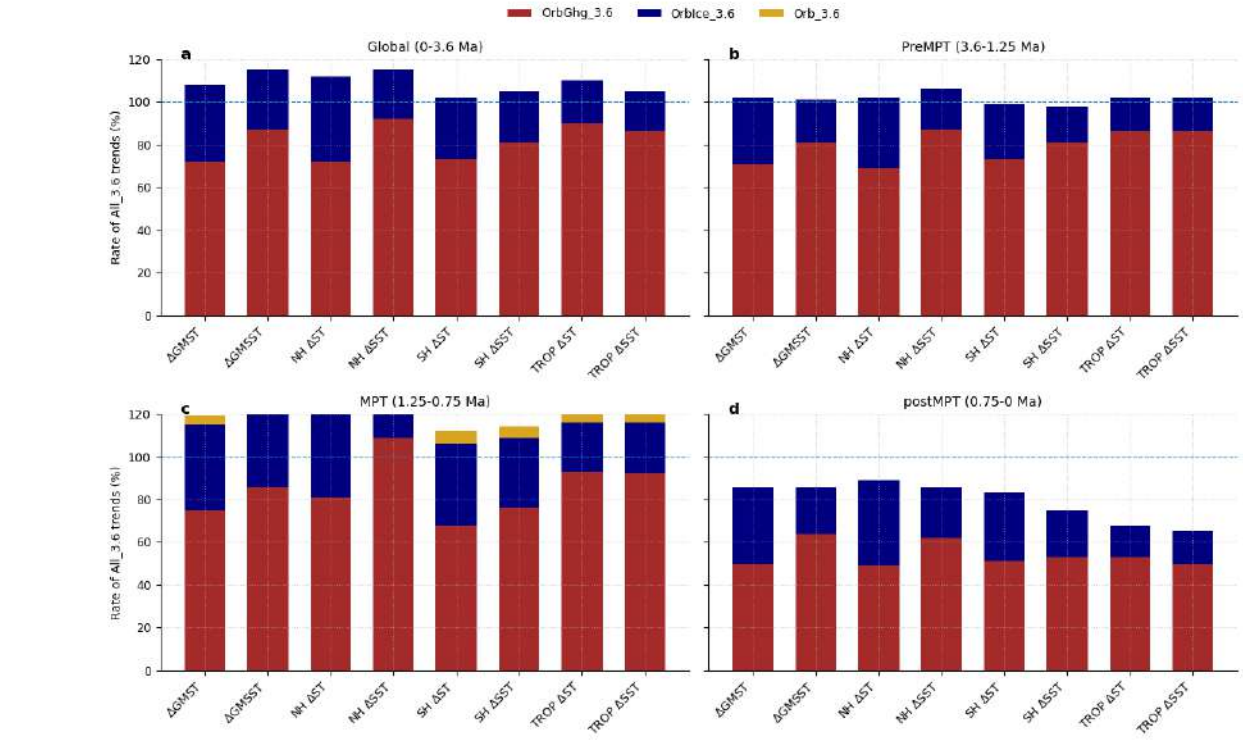

(a)

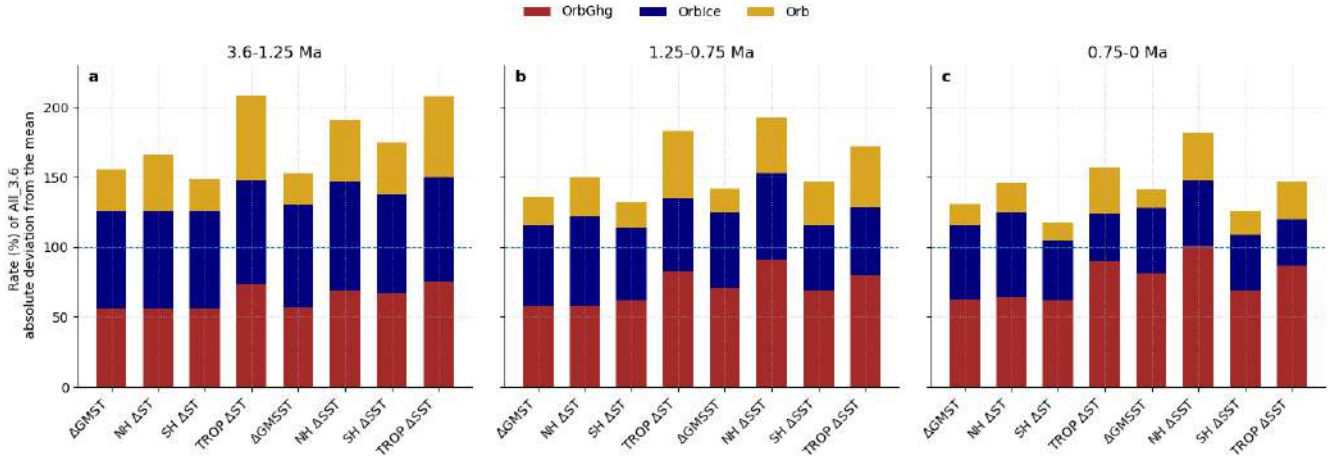

(b)

Figure 7. Relative contributions of OrbGhg (red), OrbIce (blue), and OrbOnly (yellow) to temperature variability in All_forcings. Contributions are expressed as percentages of All_forcings temperature trends (a) and mean absolute deviations from the mean (b), for global mean surface and sea surface temperatures (ΔGMST, ΔGMSST), and Northern and Southern Hemisphere surface and sea surface temperatures (NHΔST, NHΔSST, SHΔST, SHΔSST). Values are shown for 3.6–1.25 Ma, 1.25–0.75 Ma, 0.75–0 Ma, and for the full period (3.6–0 Ma) in (a). The dashed line indicates 100%, corresponding to the variability simulated in All_forcings.

https://doi.org/10.5194/egusphere-2026-3719
Preprint. Discussion started: 8 July 2026

3.2.3 Individual forcing impacts on glacial-interglacial pacing

To further investigate the impact of each forcing on glacial-interglacial variability, we decompose the temperature signals into periodic components and identify the dominant modes of variability using wavelet power spectrum analysis (Torrence and Compo, 1998) (Khider et al., 2022) (Fig.9, 10, 11, 12) and power spectrum analysis (Fig.8). In particular, power spectrum densities (PSD) of SST timeseries from our simulation sets are compared with the one from Yun et al. (2023) transient simulation. Fig.8 (b) shows ΔSST PSDs from our simulation sets, and from (Yun et al., 2023) simulation. Both at global and regional scales, PSDs from All_forcing simulation set closely match the one obtained from (Yun et al., 2023). This result indicates that no memory past orbital-paced forcings seems to dramatically impact the variability of SSTs at global and hemispheric scale, neither around the Tropics, making equilibrium simulations suitable to investigate orbital variations of the climate.

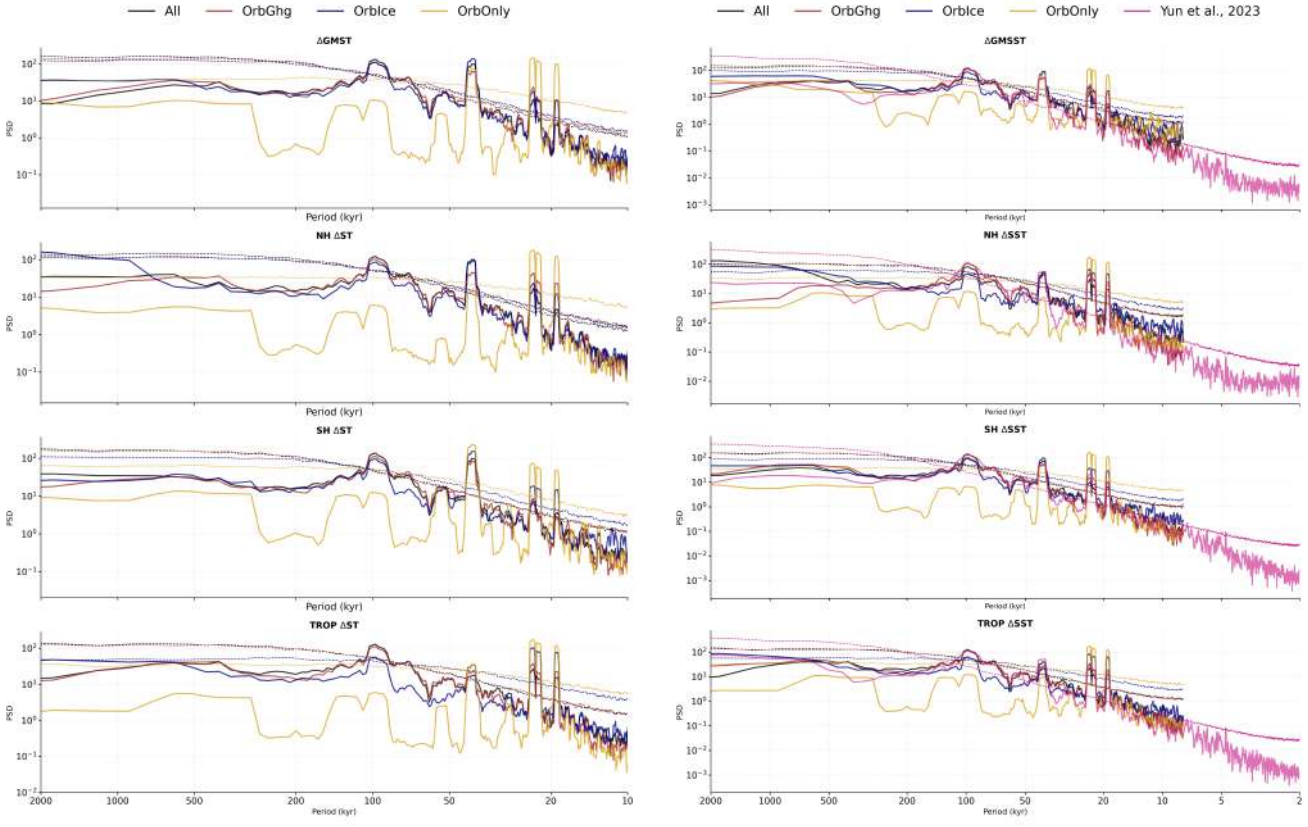

(a) (b)

Figure 8. Power spectrum densities (PSD) for air (a) and sea (b) surface temperatures. PSD are shown in plain line for All_forcings (black), OrbGhg (red), OrbIce (blue), and OrbOnly (yellow) and for the sea surface temperature from Yun et al. (2023) transient simulation (pink). Dash lines mark the 95% confidence level associated to each PSD. Analysis follows (Khider et al., 2022).

https://doi.org/10.5194/egusphere-2026-3719
Preprint. Discussion started: 8 July 2026

In terms of the evolution of the leading cycles, at the global scale, All_forcings captures the key modes of variability observed in geological records (Herbert, 2023) (Clark et al., 2024), and in (Yun et al., 2023). Wavelet spectra of ΔGMST and ΔGMSST (Fig.9; top rows) show dominant obliquity pacing over the past 3 Ma and a marked emergence of a significant 100-ka power from ≈1 Ma, marking the MPT. In addition, weaker but still significant precession-scale pacing is also emerging, from ≈1.5 Ma.

The dominant modes of variability observed in global surface temperatures from All_forcings are closely reproduced by OrbGhg (Fig.9; second rows & Fig.8), revealing that CO_2_eq forcing alone can generate the principal modes of variability on surface temperatures. Nonetheless, the wavelet power spectrum of the prescribed $CO2_2$_eq timeseries (Fig.1 (a) C) does not fully match those of ΔGMST and ΔGMSST simulated in OrbGhg, neither those of TROPΔST and TROPΔSST (Fig.12), which are more directly influenced by greenhouse gases. This suggests that the CO2_eq impact is not fully direct. In particular, the obliquity pacing diminishes when the 100-ka period of the MPT emerges, and an additional significant 100-ka periodicity is present near 3 Ma in the CO2_eq forcing but is not expressed in the simulated surface temperature spectra.

Wavelet power spectra from OrbIce show a similar, though not identical, evolution of dominant variability to All_forcings at the global scale (Fig.9; third rows). The obliquity signal is more pronounced in OrbIce ΔGMST but weaker in ΔGMSST compared to All_forcings, while precession-band power is reduced in both (Fig.8). Nevertheless, the emergence of the 100-ka periodicity occurs at a similar time in OrbIce, OrbGhg, and All_forcings, but with reduced power in OrbIce (Fig.8). OrbIce ΔGMST dominant modes of variability are similar to the one of the global ice volume timeseries (Fig.1 (b) B) while ΔGMSST differs from its weaker obliquity signal. As expected, the wavelet power spectra and power spectrum densities (PSD) and of TROPΔST and TROPΔSST in OrbIce more closely resemble those of OrbOnly (Fig.12 & Fig.8; bottom row) than those of All_forcings or OrbGhg, supporting the limited influence of ice sheet variability in the Tropics.

Generally, these results show that both greenhouse gas and ice sheet forcings can, at global scale, independently drive the shift in surface temperature cyclicity during the MPT, whereas insolation forcing alone only generates precession-band variability (Fig.9, 10, 11, 12; bottom rows).

The study of the hemispheric temperatures wavelet spectra (Fig.10, 11) offers additional insights into the mechanisms through which orbital-scale forcings influence temperature variability. Notably, obliquity-band variability is more pronounced in Southern than Northern hemisphere temperatures (Fig.8). This asymmetry is particularly evident in OrbOnly where SHΔST shows a major 40-ka cycle alongside precession variability, whereas the NHΔST is dominated by precession alone (Fig.10,11; bottom rows). The dominant role of precession in the Northern hemisphere and obliquity in the Southern hemisphere is directly observed in OrbOnly PSD (Fig.8) and is consistent with previous modelling and geological studies (Wu et al., 2020) (Timmermann et al., 2014) (Lo et al., 2018) (Cronin et al., 2013). In particular, (Wu et al., 2020) and (Timmermann et al., 2014) whom identified obliquity as a key driver of Southern hemisphere sea ice variability. Consistent with this, removing sea ice regions from our analysis eliminates the obliquity-band signal in Southern hemisphere air temperature variability (Fig.A3 (e-f)). As such, this explains why no 40-ka cycle is observed in OrbOnly SHΔSST (Fig.11; bottom row) because sea surface areas only account for temperature below sea ice cover.

https://doi.org/10.5194/egusphere-2026-3719
Preprint. Discussion started: 8 July 2026

Excluding OrbOnly, which does not produce the transition, the 100-ka signal emergence at the MPT is reproduced for all NHΔST SHΔST wavelet spectra from the three snapshot sets (Fig.10,11; first three rows), indicating an equal contribution from both hemispheres and forcings to explain global air surface temperature variability. Conversely, while both OrbGhg and OrbIce reproduce the periodicity shift in SHΔSST, only OrbGhg captures it in NHΔSST. As such, with the combination of both, All_forcings exhibits a weaker 100-ka signal for NHΔSST than for SHΔSST after the MPT (Fig.10,11; top row). These results indicate that both greenhouse gases and ice sheet variations contribute to the emergence of the 100-ka cyclicity in SHΔSST, whereas greenhouse gases appear to be the dominant driver in the Northern hemisphere.

Interestingly, the 100-ka power in the prescribed ice sheet variability arises solely from Northern hemisphere ice sheets and is absent in the Southern hemisphere (Fig.1 (b) C)). Eliminating both ice sheet and/or sea ice region in the wavelet analysis of NHΔST and SHΔST provides some indications about how the 100-ka cycle emerges in OrbIce (Fig.A3). Notably, the 100-ka power from OrbIce NHΔST vanishes when northern sea ice area are excluded, but not when the ice sheet cover is removed. Therefore, ice sheet variability drives surface temperature variations indirectly in the Northern hemisphere, through sea ice formation. Conversely, eliminating sea ice or ice sheet areas does not impact the 100-ka signal of OrbIce SHΔST. Southern hemisphere temperature variability in OrbIce is thus likely governed by internal feedback mechanisms within the climate system. Notably, previous studies have identified feedbacks between Arctic sea ice and Atlantic Meridional Overturning Circulation (AMOC) (Delworth et al., 2016) (Liu and Fedorov, 2022) and have shown that AMOC variations influence Southern temperatures through heat transport changes (Diamond et al., 2025) (Crowley, 1992). AMOC variability and inclusion of Northern-sourced water in the Southern ocean are mainly impacted by the ice sheet forcing in our simulations (not shown), suggesting its potential influence on Southern temperatures variations within OrbIce. Greenhouse gases, on the other hand have a more limited impact on AMOC variability, implying that CO_2_eq drives surface temperature variations more directly via the atmosphere. However, further investigations on the role of the ocean circulation during the MPT will be the subject of future work.

Overall, both greenhouse gases and ice sheet variations contribute to the emergence of the 100-ka cyclicity during the MPT. Greenhouse gases directly modulate the dominant modes of variability, while ice sheets seem to influence temperatures through sea ice and ocean circulation feedbacks.

https://doi.org/10.5194/egusphere-2026-3719
Preprint. Discussion started: 8 July 2026

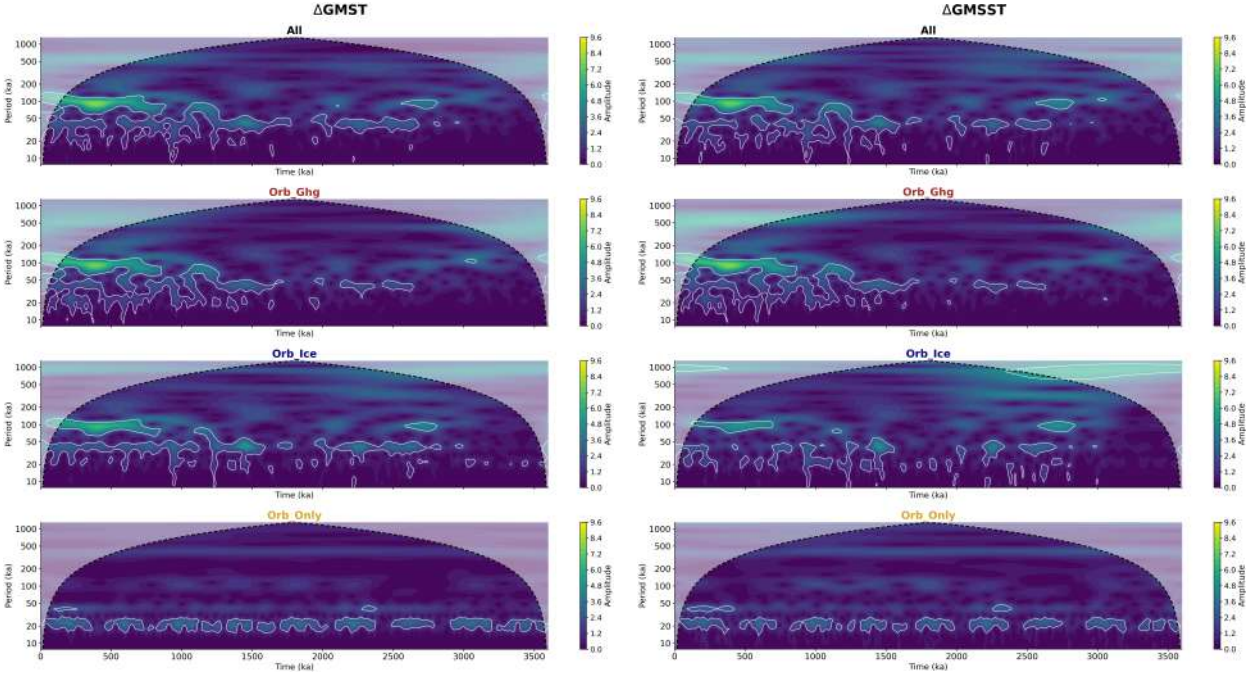

(a) (b)

Figure 9. Wavelet power spectra of global surface air and sea surface temperature variability. Spectra are shown for All_forcings (black), OrbGhg (red), OrbIce (blue), and OrbOnly (yellow), based on the timeseries in Fig.(3). Surface temperature: ΔGMST (a). Sea surface temperature: ΔGMSST (b). Analysis follows (Khider et al., 2022), white coutour depicts regions at the 95% confidence level relative to a red-noise process and the shaded regions denote the cone of influence of the mother wavelet.

https://doi.org/10.5194/egusphere-2026-3719
Preprint. Discussion started: 8 July 2026

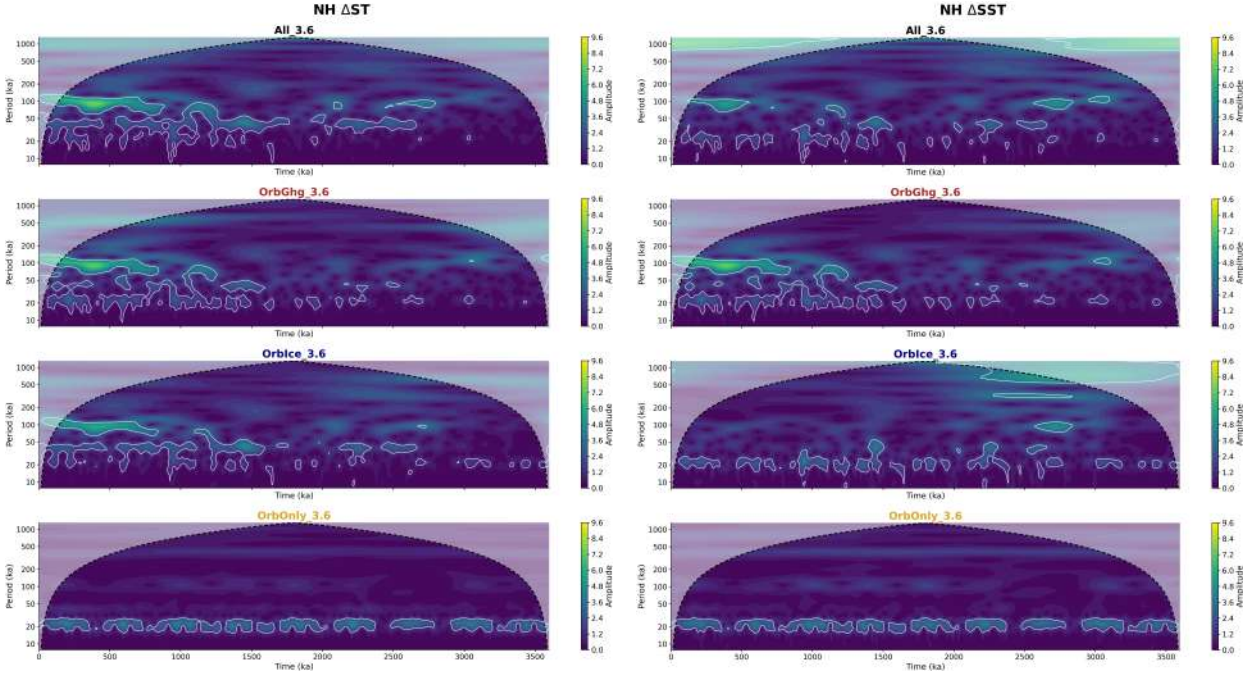

(a) (b)

Figure 10. Wavelet power spectra of Northern hemisphere surface air and sea surface temperature variability in the Northern Hemisphere. Spectra are shown for All_forcings (black), OrbGhg (red), OrbIce (blue), and OrbOnly (yellow), based on the timeseries in Fig.(4). Surface temperature: NHΔST (a). Sea surface temperature: NHΔSST (b). Analysis follows (Khider et al., 2022), white coutour depicts regions at the 95% confidence level relative to a red-noise process and the shaded regions denote the cone of influence of the mother wavelet.

https://doi.org/10.5194/egusphere-2026-3719
Preprint. Discussion started: 8 July 2026

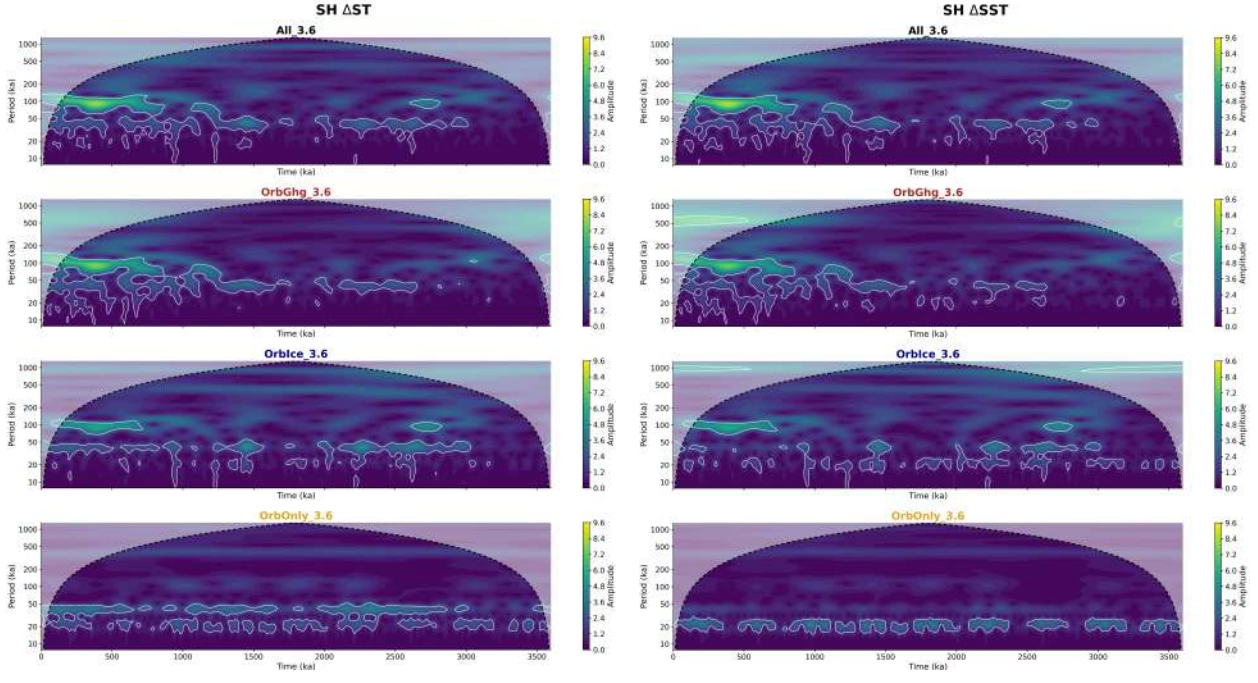

(a) (b)

Figure 11. Wavelet power spectra of Southern hemisphere surface air and sea surface temperature variability in the Southern Hemisphere. Spectra are shown for All_forcings (black), OrbGhg (red), OrbIce (blue), and OrbOnly (yellow), based on the timeseries in Fig.(5). Surface temperature: SHΔST (a). Sea surface temperature: SHΔSST (b). Analysis follows (Khider et al., 2022), white coutour depicts regions at the 95% confidence level relative to a red-noise process and the shaded regions denote the cone of influence of the mother wavelet.

https://doi.org/10.5194/egusphere-2026-3719
Preprint. Discussion started: 8 July 2026

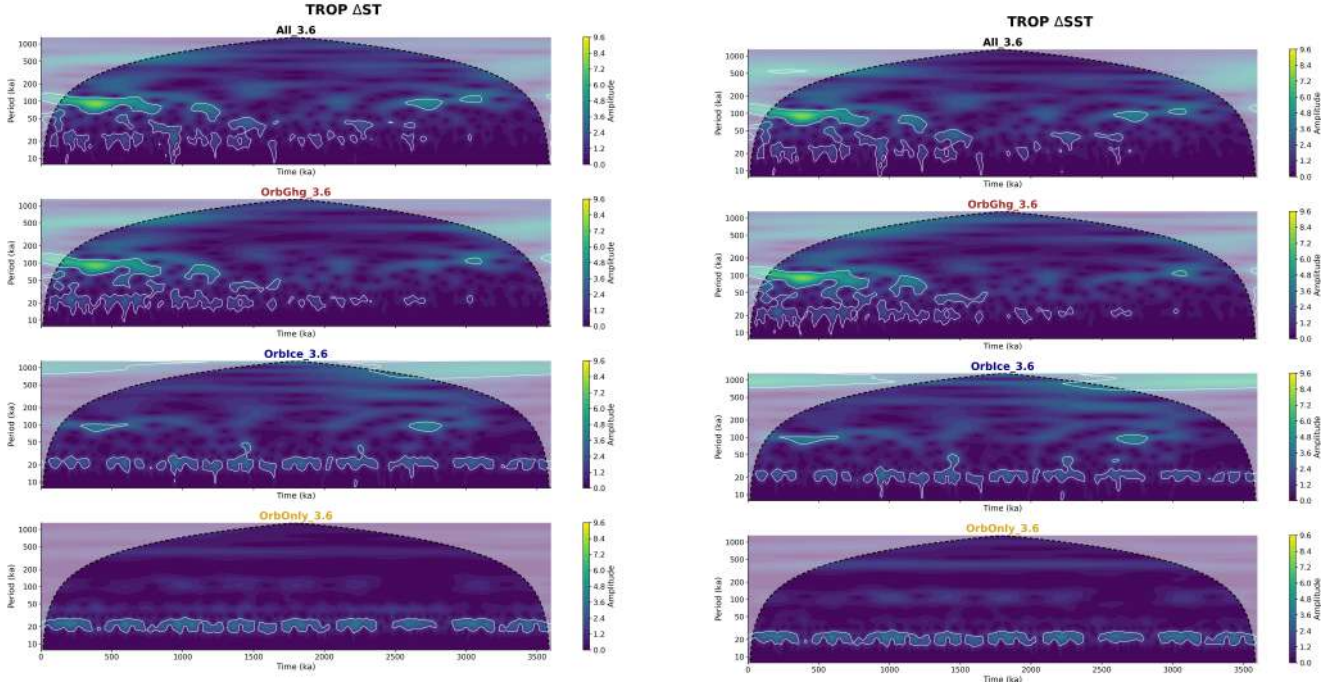

(a) (b)

Figure 12. Wavelet power spectra of tropical surface air and sea surface temperature variability in the tropics. Spectra are shown for All_forcings (black), OrbGhg (red), OrbIce (blue), and OrbOnly (yellow), based on the timeseries in Fig.(6). Surface temperature: TROPΔST (a). Sea surface temperature: TROPΔSST (b). Analysis follows (Khider et al., 2022), white coutour depicts regions at the 95% confidence level relative to a red-noise process and the shaded regions denote the cone of influence of the mother wavelet.

https://doi.org/10.5194/egusphere-2026-3719
Preprint. Discussion started: 8 July 2026

4 Discussion & Conclusion

We do not know of any change in external forcing that can explain the MPT, and hence it is generally attributed to internal feedbacks within the Earth system, involving interactions between ice sheet and greenhouse gases cycles (Herbert, 2023). The mechanisms proposed to explain a change in feedbacks that could have contributed to trigger the MPT has been detailed in (Berends et al., 2021b). Among them, changes in ice sheet stability and sensitivity to insolation has been highlighted, as well as its positive feedback on temperature and CO_2 drawdown (Tzedakis et al., 2017) (Chalk et al., 2017). Other mechanisms involve regolith erosion (Clark and Pollard, 1998) (Ganopolski and Calov, 2011) (Willeit et al., 2019) and its impact on ocean productivity and albedo (Chalk et al., 2017) (Hines et al., 2024), changes in ocean circulation and sea ice cover that could have had important feedbacks on CO_2 and continental ice volume (Menviel, 2019).

The simulations presented here reproduce the long-term global cooling trend recorded in proxy archives over the past 3.6 Ma and capture the MPT, including an acceleration of cooling, an increase in the amplitude of glacial–interglacial variability, and a shift in dominant periodicity from 40 ka to 100 ka as an emergent feature. This is an inherent outcome due to incorporating realistic boundary conditions that include the MPT shift in their variations (both our greenhouse gas and ice sheet forcing exhibit changes during the MPT). Moreover, our separation of the "forcings" into orbit, CO_2 and ice sheets is an arbitrary division of the Earth system which does not account for the feedbacks between one another. Therefore, understanding the physical processes that drive changes in greenhouse gases and ice sheet at the MPT, and evaluate which feedback has been the main trigger of the transition, is out of the scope of this study. However, our simulations do allow us to quantify the contributions of ice sheets and greenhouse gases to surface temperature variations and hence can help orient feedback explorations.

We identified in particular a dominant and direct role of greenhouse gases on surface temperature trends and glacial-interglacial variability during the MPT, aligning with (Clark et al., 2024), (Herbert, 2023) and (Willeit et al., 2019). The ice sheet impact on surface temperatures appears more modest, in agreement with (Shakun, 2017) and (Stap et al., 2019), although its contribution is still significant through sea ice formation and changes in ocean circulation, both critical to carbon storage (Marzocchi and Jansen, 2019) (Shin et al., 2003) (Ferrari et al., 2014). However, whether these processes can generate sufficient CO_2 drawdown to explain the temperature changes remains unclear. Future work focusing on the impact of changes in ocean circulation, especially convection in the Southern ocean and its role on CO_2 sequestration will provide valuable insights, following the arguments of previous studies (An et al., 2024) (Pena and Goldstein, 2014) (Hasenfratz et al., 2019) (Hines et al., 2024) (Farmer et al., 2019).

This sensitivity study also highlights how surface temperature variations are reliant on the boundary conditions applied to the model, and how this dependence evolves through time. As such, the uncertainties of our results arise from the choice of CO_2 and ice sheet forcings and associated sea-level change. In particular, given the dominant role of the greenhouse gases in driving surface temperature variations (Fig.7, Fig.9, 10, 11, 12), the choice of CO_2 reconstruction could substantially influence the simulated temperature response, particularly so when considering the palaeoclimate models climate sensitivity. This highlights the importance of the forthcoming results from the Beyond-EPICA ice core project in providing accurate longer-term CO_2 data.

https://doi.org/10.5194/egusphere-2026-3719
Preprint. Discussion started: 8 July 2026

For comparison, CO_2 concentration timeseries from (Berends et al., 2021a) matches the CO_2 levels obtained by (Köhler, 2023) using the global carbon cycle model BICYCLE under scenarios assuming a relatively slow decline in volcanic CO_2 outgassing between 4.5 and 1 Ma (2% of the long-term decline). In contrast, our CO_2_eq, as the one proposed by (Willeit et al., 2019), falls within the range of scenarios presented by (Köhler, 2023) that assume a stronger reduction in volcanic outgassing (6% of the long-term decline over the same interval). (Köhler, 2023) identified scenarios with the slowest decline in volcanic CO_2 outgassing as the most plausible. However, in light of the late Pliocene cold bias (Fig.2), the use of lower CO_2 concentrations could have further increased the discrepancy between the model and geological reconstructions. Accordingly, the recent CO_2 reconstruction of (Marks-Peterson et al., 2026), indicating only a modest decline in CO_2 ($\approx$ 20ppm) from the past 3 Ma to the pre-industrial, would not allow the model to reproduce the Pliocene temperatures reported by (Clark et al., 2024). The CO_2_eq reconstruction used here follows the framework proposed by PlioMIP (Haywood et al., 2024), which allows climate models to reach the warm Pliocene temperatures, while remaining plausible as it lies within the uncertainty range of (De La Vega et al., 2020).

Furthermore, the model does not represent potential sporadic inputs of methane in the atmosphere neither dust fluxes or sulphate aerosols inputs, despite evidence suggesting that these factors may have influenced the MPT (Panieri et al., 2023) (Martínez-Garcia et al., 2011) (Köhler, 2023). These factors are not fully constrained by geological reconstructions (Herbert, 2023), and could represent a significant missing component in our simulations which may explain the discrepancy between our simulated temperature variations and (Clark et al., 2024) temperature reconstructions.

Moreover, we showed that land ice sheet volume and extent plays an important role to explain the amplitude of the glacial-interglacial variability (Fig.7 (b)). As such, a different choice of ice sheet reconstruction could have also significantly impacted our results. In particular, our comparison against (Yun et al., 2023), shows that an alternative ice sheet reconstruction prescribing lower sea levels than de (De Boer et al., 2014) over the last 800-ka, such as (Willeit et al., 2019) (Fig.1 (a) B)), could have helped the model better reproduce the glacial temperatures. In addition, the recently published reconstruction of global mean sea level from (Clark et al., 2025a) supports that (De Boer et al., 2014) reconstruction might have underestimated ice sheet volume and/or extent during glacial periods due to sea levels not falling enough over the past 800-ka (Fig.1 (a) B)). In future, we hope to repeat our simulations with the (Willeit et al., 2019) reconstruction. However, our simulations represent a huge computational effort and we will need to seek additional resource.

The differences between our "snapshot" and the "accelerated" transient simulation presented in (Yun et al., 2023) might also arise from the difference in the methodology chosen to run the simulation. The "snapshot" simulations used in this study are one method to allow fully coupled models to address long term climate variability. They have the benefit of having clearly defined physics, but assume that the climate is approximately in balance with the forcings and is independent of the initial conditions. An unpublished comparison of a transient 26ka - 0ka HadCM3 simulation with "snapshots" suggests that these approximations are relatively good (errors in global mean temperature generally less than 0.5 ^{o}C) but other time periods may be different. "Accelerated" transient simulations such as (Yun et al., 2023) have the benefit that the model "knows" about previous states and does not assume equilibrium conditions. However, the interaction between the forcing and climate response could be potentially distorted sense, the impact of which is not fully understood i.e. a 5x acceleration means that precessional forcing is

https://doi.org/10.5194/egusphere-2026-3719
Preprint. Discussion started: 8 July 2026

occurring on a 4000 year period, which is artificially close to the intrinsic deep ocean time scale (1000-2000 years). This could potentially lead to unusual vertical density gradients and unrealistic ocean circulation changes (Lunt et al., 2006) (Varma et al., 2016). Our comparison to (Yun et al., 2023) is inclusive as whether "acceleration" or "snapshots" is better.

Prior to the past 800 ka, both sea level timeseries from (De Boer et al., 2014) and from (Willeit et al., 2019) substantially differ from (Clark et al., 2025a) reconstruction, which exhibits the onset of the late Quaternary glacial-interglacial amplitude from ≈3 Ma (Fig.1 (a) B)) while in most other reconstructions, late Quaternary glaciation levels only appear at the MPT, not before. As this new reconstruction has not been applied as a forcing in climate model simulations to date, a direct comparison of its effects on global climate with those of the reconstruction used in this study (De Boer et al., 2014) is not possible. However, analysis of OrbIce series suggest that the increase in ice sheet extent at the MPT is sufficient enough to drive a cooling trend, and is an important contributor of the complete trend observed in All_forcings (Fig.3, 4, 5 and 6). As such, prescribing the onset of Quaternary ice sheets at 3 Ma would likely have enhanced cooling, potentially increasing the discrepancy between simulated temperatures and geological reconstructions. In addition, changes in ice sheet volume can impact ocean overturning circulation (not shown), for example, increasing variability of the AMOC from the MPT in our simulations. This result aligns with the hypothesis that ocean circulation changes contributed to the MPT, via increasing carbon burial in the ocean (Chalk et al., 2017) (An et al., 2024) (Berends et al., 2021b) (Pena and Goldstein, 2014) (Farmer et al., 2019). An earlier onset of Quaternary ice sheets at 3 Ma as proposed by (Clark et al., 2025a), would likely have led to an earlier intensification in the simulations of AMOC variability accordingly, rather than as seen during the MPT. As such, apart for the last 800-ka, the global mean sea-level reconstruction of (Clark et al., 2025a) is likely to be insufficient to improve model agreement with the geological archives.

In addition, in reconstructing sea level evolution, (Clark et al., 2025a) assumed that the relationship between global mean ocean temperature (GMOT) and global mean SST (GMSST) evolved across the MPT, with a GMOT/GMSST ratio of 50% before the MPT and 1 thereafter, revealing an increase in ocean heat uptake, as argued in (Clark et al., 2025b). Our All_forcings set reveals an evolution in GMOT/GMSST ratio over the MPT, but not in the extent proposed by (Clark et al., 2025a): we obtain a ratio of GMOT/GMSST = 0.87 prior the MPT (3.6 - 1.25 Ma), which increases during and after the MPT to reach 1.1 (Fig.S4 & Tab.S3). The other simulation sets suggest an opposite behaviour; larger GMOT/GMSST ratio before the MPT than after (Fig.A4 & Tab.A3). Nevertheless, temperature variability (both GMOT and GMSST) is weaker than in All_forcings, which complicates the interpretation of these results.

Overall, the simulations presented in this work suggest that further improvements on CO_2 and ice sheet reconstructions, as well as model climate sensitivity, are required to improve model-data agreement. This, in turn, will help constrain the roles of these forcings and orient the exploration of feedbacks between them, notably during the MPT.

5 Author contributions

Paul Valdes designed the experiments. Paul Valdes and Jeanne Millot-Weil ran the simulation sets. Jeanne Millot-Weil performed the analysis and prepared the manuscript with contributions from all co-authors.

https://doi.org/10.5194/egusphere-2026-3719
Preprint. Discussion started: 8 July 2026

Appendix A

PreMPT (3.6 Ma - 1250 ka)	All_forcings	OrbGhg	OrbIce	OrbOnly
ΔGMST	0.54	0.30 (56% of All_forc)	0.38 (70% of All_forc)	0.16 (30% of All_forc)
ΔGMSST	0.30	0.17 (57%)	0.22 (73%)	0.07 (23%)
NH ΔST	0.68	0.39 (56%)	0.51 (70%)	0.27 (40%)
NH ΔSST	0.36	0.25 (69%)	0.28 (78%)	0.16 (44%)
SH ΔST	0.43	0.24 (56%)	0.30 (70%)	0.10 (23%)
SH ΔSST	0.24	0.16 (67%)	0.17 (71%)	0.09 (37%)
TROP ΔST	0.31	0.23 (74%)	0.23 (74%)	0.19 (61%)
TROP ΔSST	0.24	0.18 (75%)	0.18 (75%)	0.14 (58%)
MPT (1250 - 750 ka)	All_forcings	OrbGhg	OrbIce	OrbOnly
ΔGMST	0.80	0.46 (58% of All_forc)	0.46 (58% of All_forc)	0.16 (20% of All_forc)
ΔGMSST	0.41	0.29 (71%)	0.22 (54%)	0.07 (17%)
NH ΔST	1.04	0.59 (58%)	0.67 (64%)	0.29 (28%)
NH ΔSST	0.42	0.38 (91%)	0.26 (62%)	0.17 (40%)
SH ΔST	0.56	0.35 (62%)	0.29 (52%)	0.10 (18%)
SH ΔSST	0.32	0.22 (69%)	0.15 (47%)	0.10 (31%)
TROP ΔST	0.42	0.35 (83%)	0.22 (52%)	0.20 (48%)
TROP ΔSST	0.35	0.28 (80%)	0.17 (49%)	0.15 (43%)
postMPT (750 ka - 0)	All_forcings	OrbGhg	OrbIce	OrbOnly
ΔGMST	1.10	0.69 (63% of All_forc)	0.58 (53% of All_forc)	0.16 (15% of All_forc)
ΔGMSST	0.53	0.43 (81%)	0.25 (47%)	0.07 (13%)
NH ΔST	1.32	0.84 (64%)	0.81 (61%)	0.28 (21%)
NH ΔSST	0.47	0.50 (101%)	0.22 (47%)	0.16 (34%)
SH ΔST	0.88	0.55 (62%)	0.38 (43%)	0.11 (13%)
SH ΔSST	0.52	0.36 (69%)	0.21 (40%)	0.09 (17%)
TROP ΔST	0.58	0.52 (90%)	0.20 (34%)	0.19 (33%)
TROP ΔSST	0.48	0.42 (87%)	0.16 (33%)	0.13 (27%)

Table A1. Mean absolute deviation (°C) from the mean for temperatures from each snapshot set (All_forcings, OrbGhg, OrbIce and OrbOnly) ($\overline{abs\_deviation} = |TS_{detrend} - \overline{TS\_detrend}|$). Percentages indicate the fraction of variability relative to All_forcings within each time interval: 3.6–1.25 Ma (prior to MPT), 1.25–0.75 Ma (during the MPT) and 0.75–0 Ma (after the MPT).

https://doi.org/10.5194/egusphere-2026-3719
Preprint. Discussion started: 8 July 2026

Global (0 - 3.6 Ma)	All_forcings	OrbGhg	OrbIce	OrbOnly
ΔGMST	-1.49	-1.08 (72% of All_forc)	-0.53 (36% of All_forc)	0.0
ΔGMSST	-0.78	-0.68 (87%)	-0.22 (28%)	0.0
NH ΔST	-1.84	-1.32 (72%)	-0.72 (40%)	0.0
NH ΔSST	-0.88	-0.81 (92%)	-0.20 (23%)	0.0
SH ΔST	-1.11	-0.83 (73%)	-0.32 (29%)	0.0
SH ΔSST	-0.68	-0.55 (81%)	-0.16 (24%)	0.0
TROP ΔST	-0.96	-0.86 (90%)	-0.19 (20%)	0.0
TROPΔSST	-0.78	-0.67 (86%)	-0.15 (19%)	0.0
PreMPT (3.6 Ma - 1250 ka)	All_forcings	OrbGhg	OrbIce	OrbOnly
ΔGMST	-1.61	-1.14 (71% of All_forc)	-0.50 (31% of All_forc)	0.0
ΔGMSST	-0.80	-0.65 (81%)	-0.16 (20%)	0.0
NH ΔST	-2.03	-1.40 (69%)	-0.68 (33%)	0.0
NH ΔSST	-1.01	-0.87 (87%)	-0.19 (19%)	0.0
SH ΔST	-1.17	-0.86 (73%)	-0.30 (26%)	0.0
SH ΔSST	-0.70	-0.57 (81%)	-0.12 (17%)	0.0
TROP ΔST	-1.08	-0.93 (86%)	-0.17 (16%)	0.0
TROPΔSST	-0.83	-0.71 (86%)	-0.13 (16%)	0.0
MPT (1250 - 750 ka)	All_forcings	OrbGhg	OrbIce	OrbOnly
ΔGMST	-2.88	-2.17 (75% of All_forc)	-1.16 (40% of All_forc)	-0.12 (4% of All_forcings)
ΔGMSST	-1.55	-1.34 (86%)	-0.55 (35%)	0.05 (3%)
NH ΔST	-3.23	-2.62 (81%)	-1.34 (41%)	-0.10 (3%)
NH ΔSST	-1.46	-1.59 (109%)	-0.34 (23%)	-0.06 (4%)
SH ΔST	-2.48	-1.70 (68%)	-0.94 (38%)	-0.14 (6%)
SH ΔSST	-1.48	-1.12 (76%)	-0.49 (33%)	-0.08 (5%)
TROP ΔST	-1.74	-1.62 (93%)	-0.40 (23%)	-0.07 (4%)
TROP ΔSST	-1.45	-1.33 (92%)	-0.35 (24%)	-0.07 (5%)
postMPT (750 ka - 0)	All_forcings	OrbGhg	OrbIce	OrbOnly
ΔGMST	0.66	0.33 (50% of All_forc)	0.24 (36% of All_forc)	0.0
ΔGMSST	0.31	0.20 (64%)	0.07 (22%)	0.0
NH ΔST	0.78	0.38 (49%)	0.31 (40%)	0.0
NH ΔSST	0.37	0.23 (62%)	0.09 (24%)	0.0
SH ΔST	0.53	0.27 (51%)	0.17 (32%)	0.0
SH ΔSST	0.32	0.17 (53%)	0.07 (22%)	0.0
TROP ΔST	0.40	0.21 (53%)	0.06 (15%)	0.0
TROP ΔSST	0.34	0.17 (50%)	0.05 (15%)	0.0

Table A2. Temperature trend slopes relative to All_forcings Slopes (in °C/Ma) for each simulation set (All_forcings, OrbGhg, OrbIce and OrbOnly). Percentages indicate the fraction of variability relative to All_forcings within each time interval: 3.6–1.25 Ma (prior to MPT), 1.25–0.75 Ma (during the MPT) and 0.75–0 Ma (after the MPT).

https://doi.org/10.5194/egusphere-2026-3719
Preprint. Discussion started: 8 July 2026

	Pre MPT (3.6 Ma - 1250 ka)	MPT (1250 - 750 ka)	Post MPT (750 ka - 0 BP)
All_forcings	0.87	1.1	1.1
OrbGhg	1.3	0.65	0.92
OrbIce	1.3	1.3	0.46
OrbOnly	1.1	0.60	0.58

Table A3. Global mean ocean temperature (GMOT) and global mean sea surface temperature (GMSST) ratios. Ratios calculated for each time interval: 3.6–1.25 Ma (prior to MPT), 1.25–0.75 Ma (during the MPT) and 0.75–0 Ma (after the MPT), and for each simulation sets (All_forcings, OrbGhg, OrbIce and OrbOnly).

https://doi.org/10.5194/egusphere-2026-3719
Preprint. Discussion started: 8 July 2026

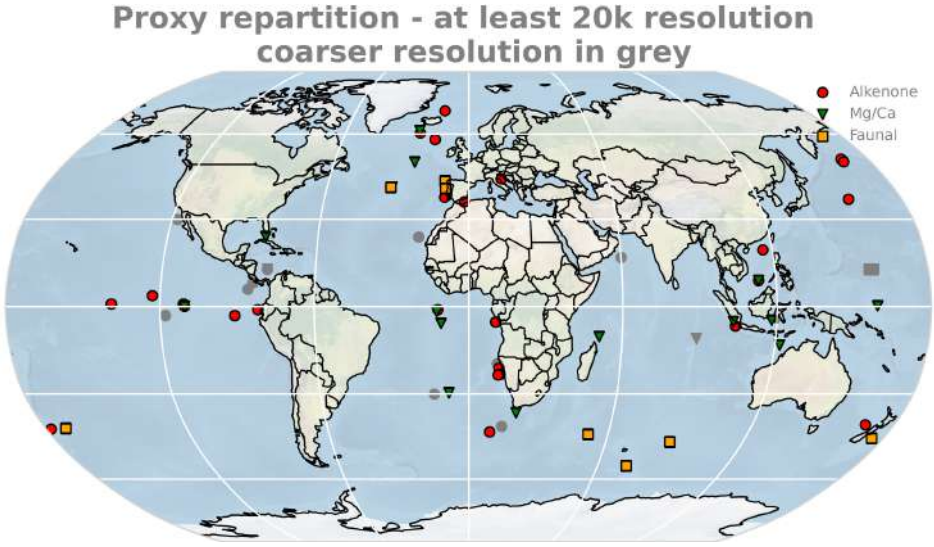

Figure A1. Location of the geological archives used by (Clark et al., 2024) to build the stacks. Archives with 20 ka of resolution or higher are shown in colour, coarser records are in grey.

https://doi.org/10.5194/egusphere-2026-3719
Preprint. Discussion started: 8 July 2026

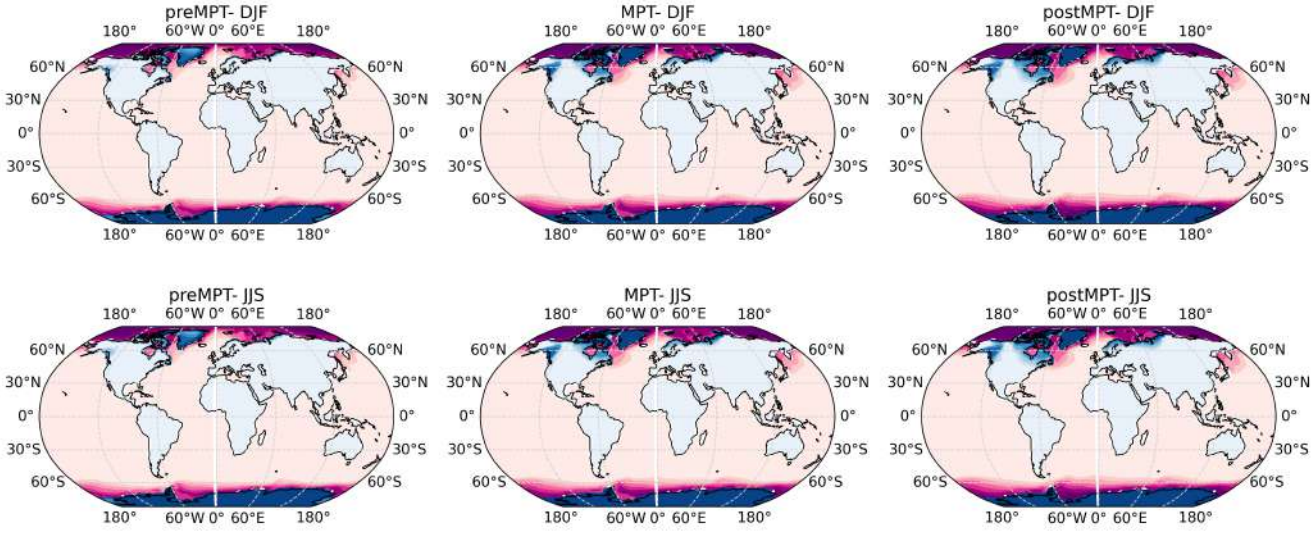

Figure A2. Ice sheet and sea ice cover evolution before, during and after the MPT in All_forcings. Ice sheet and sea ice cover are averaged over the time period of interest, top row: in winter (december to february - DJF) and bottom row: in summer (June to September - JJS).

https://doi.org/10.5194/egusphere-2026-3719
Preprint. Discussion started: 8 July 2026

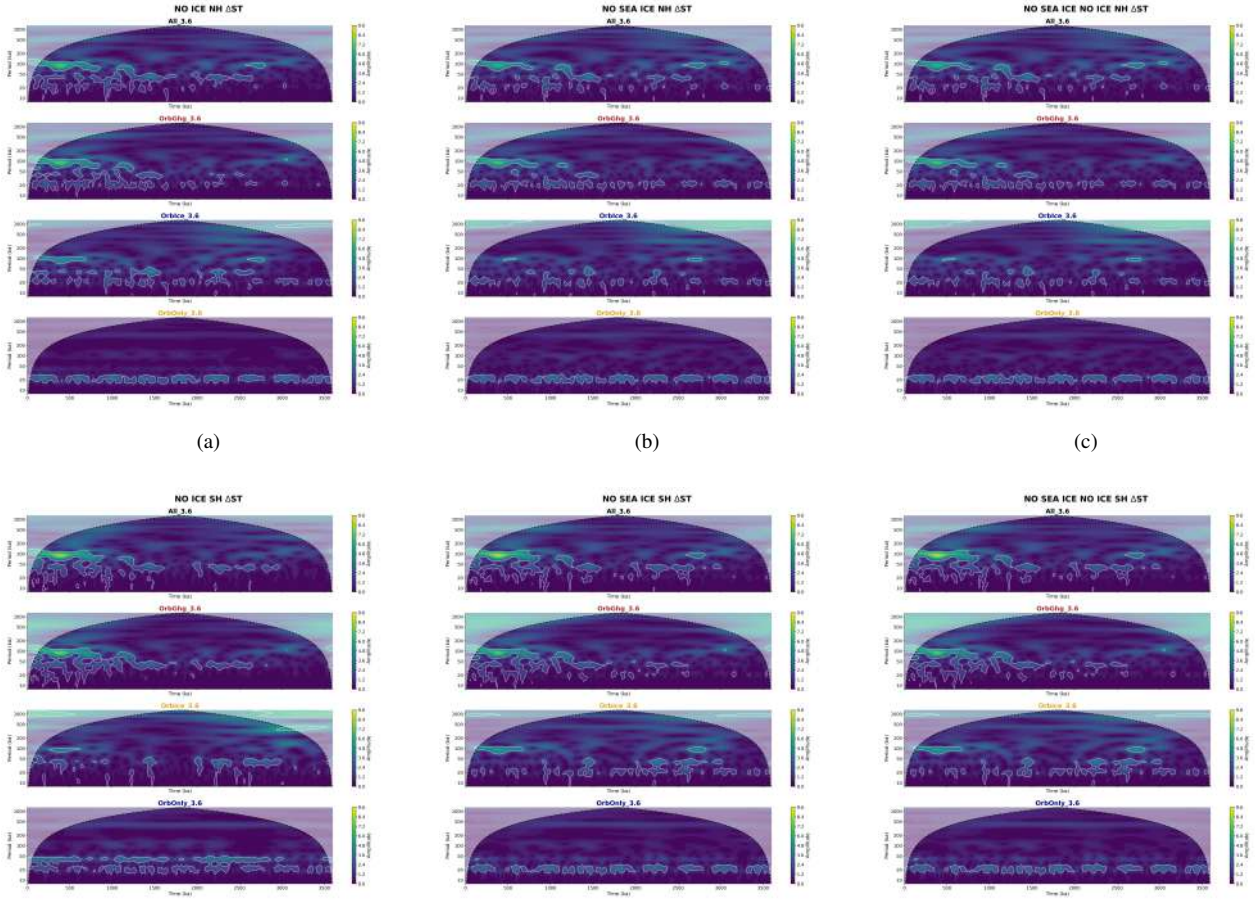

Figure A3. Wavelet power spectra of Northern and Southern surface air temperature variability without ice sheet cover and/or sea ice cover. Spectra are shown for All_forcings (black), OrbGhg (red), OrbIce (blue), and OrbOnly (yellow). (a & d) show spectra without ice sheet cover, (b & e) without sea ice cover and (c & f) without either ice sheet or sea ice cover.

https://doi.org/10.5194/egusphere-2026-3719
Preprint. Discussion started: 8 July 2026

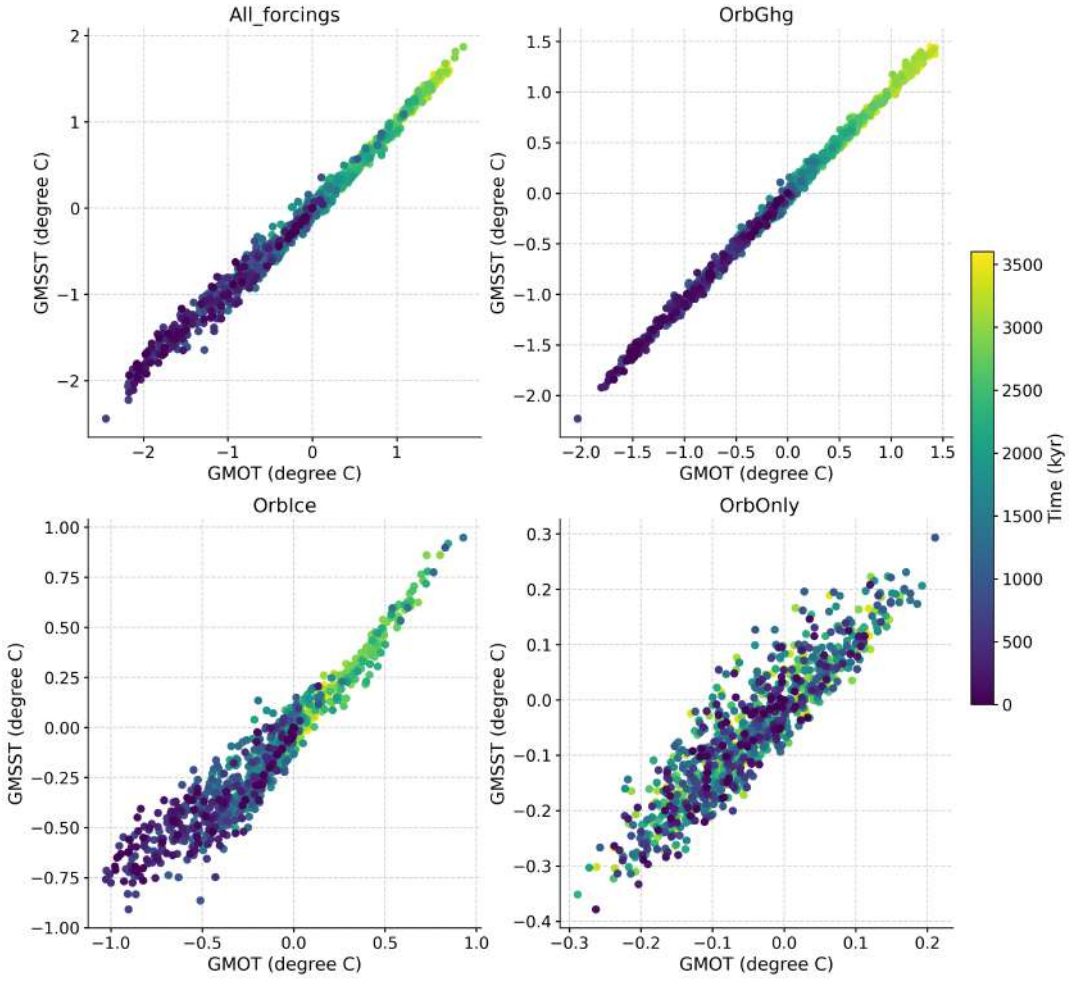

Figure A4. Global mean ocean temperature (GMOT) vs global mean sea surface temperature (GMSST), annual mean. Relationship is shown for All_forcings (top left), OrbGhg (top right), OrbIce (bottom left) and OrbOnly (bottom right).

Competing interests. The authors declare no competing interests.

https://doi.org/10.5194/egusphere-2026-3719
Preprint. Discussion started: 8 July 2026

References

Abe-Ouchi, A., Saito, F., Kageyama, M., Braconnot, P., Harrison, S. P., Lambeck, K., Otto-Bliesner, B. L., Peltier, W. R., Tarasov, L., Peterschmitt, J.-Y., and Takahashi, K.: Ice-sheet configuration in the CMIP5/PMIP3 Last Glacial Maximum experiments, Geoscientific Model Development, 8, 3621–3637, https://doi.org/10.5194/gmd-8-3621-2015, 2015.

Ahn, S., Khider, D., Lisiecki, L. E., and Lawrence, C. E.: A probabilistic Pliocene–Pleistocene stack of benthic δ18O using a profile hidden Markov model, Dynamics and Statistics of the Climate System, 2, https://doi.org/10.1093/climsys/dzx002, 2017.

An, Z., Zhou, W., Zhang, Z., Zhang, X., Liu, Z., Sun, Y., Clemens, S. C., Wu, L., Zhao, J., Shi, Z., Ma, X., Yan, H., Li, G., Cai, Y., Yu, J., Sun, Y., Li, S., Zhang, Y., Stepanek, C., Lohmann, G., Dong, G., Cheng, H., Liu, Y., Jin, Z., Li, T., Hao, Y., Lei, J., and Cai, W.: Mid-Pleistocene climate transition triggered by Antarctic Ice Sheet growth, Science, 385, 560–565, https://doi.org/10.1126/science.abn4861, 2024.

Armstrong, E., Hopcroft, P. O., and Valdes, P. J.: A simulated Northern Hemisphere terrestrial climate dataset for the past 60,000 years, Scientific Data, 6, 265, https://doi.org/10.1038/s41597-019-0277-1, 2019.

Armstrong, E., Tallavaara, M., Hopcroft, P. O., and Valdes, P. J.: North African humid periods over the past 800,000 years, Nature Communications, 14, 5549, https://doi.org/10.1038/s41467-023-41219-4, 2023.

Berends, C. J., de Boer, B., and Wal, R. S. W. v. d.: Reconstructing the evolution of ice sheets, sea level, and atmospheric \chemCO_2 during the past 3.6 million years, Climate of the Past, 17, 361–377, https://doi.org/10.5194/cp-17-361-2021, 2021a.

Berends, C. J., Köhler, P., Lourens, L. J., and Van De Wal, R. S. W.: On the Cause of the Mid-Pleistocene Transition, Reviews of Geophysics, 59, e2020RG000 727, https://doi.org/10.1029/2020RG000727, 2021b.

Berger, A., Loutre, M. F., and Gallée, H.: Sensitivity of the LLN climate model to the astronomical and CO 2 forcings over the last 200 ky, Climate Dynamics, 14, 615–629, https://doi.org/10.1007/s003820050245, 1998.

Broccoli, A. J.: Tropical Cooling at the Last Glacial Maximum: An Atmosphere–Mixed Layer Ocean Model Simulation, Journal of Climate, 13, 951–976, https://doi.org/10.1175/1520-0442(2000)013<0951:TCATLG>2.0.CO;2, 2000.

Chalk, T. B., Hain, M. P., Foster, G. L., Rohling, E. J., Sexton, P. F., Badger, M. P. S., Cherry, S. G., Hasenfratz, A. P., Haug, G. H., Jaccard, S. L., Martínez-García, A., Pälike, H., Pancost, R. D., and Wilson, P. A.: Causes of ice age intensification across the Mid-Pleistocene Transition, Proceedings of the National Academy of Sciences, 114, 13 114–13 119, https://doi.org/10.1073/pnas.1702143114, 2017.

Clark, P. U. and Pollard, D.: Origin of the Middle Pleistocene Transition by ice sheet erosion of regolith, Paleoceanography, 13, 1–9, https://doi.org/10.1029/97PA02660, 1998.

Clark, P. U., Archer, D., Pollard, D., Blum, J. D., Rial, J. A., Brovkin, V., Mix, A. C., Pisias, N. G., and Roy, M.: The middle Pleistocene transition: characteristics, mechanisms, and implications for long-term changes in atmospheric pCO2, Quaternary Science Reviews, 25, 3150–3184, https://doi.org/10.1016/j.quascirev.2006.07.008, 2006.

Clark, P. U., Shakun, J. D., Rosenthal, Y., Köhler, P., and Bartlein, P. J.: Global and regional temperature change over the past 4.5 million years, Science, 383, 884–890, https://doi.org/10.1126/science.adi1908, 2024.

Clark, P. U., Shakun, J. D., Rosenthal, Y., Pollard, D., Hostetler, S. W., Köhler, P., Bartlein, P. J., Gregory, J. M., Zhu, C., Schrag, D. P., Liu, Z., and Pisias, N. G.: Global mean sea level over the past 4.5 million years, Science, 390, eadv8389, https://doi.org/10.1126/science.adv8389, 2025a.

Clark, P. U., Shakun, J. D., Rosenthal, Y., Zhu, C., Bartlein, P. J., Gregory, J. M., Köhler, P., Liu, Z., and Schrag, D. P.: Mean ocean temperature change and decomposition of the benthic δ^{18} O record over the past 4.5 million years, Climate of the Past, 21, 973–1000, https://doi.org/10.5194/cp-21-973-2025, 2025b.

https://doi.org/10.5194/egusphere-2026-3719
Preprint. Discussion started: 8 July 2026

Cox, P.: Description of the TRIFFID dynamic global vegetation model, 2001.

Cronin, T., Polyak, L., Reed, D., Kandiano, E., Marzen, R., and Council, E.: A 600-ka Arctic sea-ice record from Mendeleev Ridge based on ostracodes, Quaternary Science Reviews, 79, 157–167, https://doi.org/10.1016/j.quascirev.2012.12.010, 2013.

Crowley, T. J.: North Atlantic Deep Water cools the southern hemisphere, Paleoceanography, 7, 489–497, https://doi.org/10.1029/92PA01058, 1992.

Davies-Barnard, T., Valdes, P. J., Jones, C. D., and Singarayer, J. S.: Sensitivity of a coupled climate model to canopy interception capacity, Climate Dynamics, 42, 1715–1732, https://doi.org/10.1007/s00382-014-2100-1, 2014.

De Boer, B., Lourens, L. J., and Van De Wal, R. S.: Persistent 400,000-year variability of Antarctic ice volume and the carbon cycle is revealed throughout the Plio-Pleistocene, Nature Communications, 5, 2999, https://doi.org/10.1038/ncomms3999, 2014.

De Garidel-Thoron, T., Rosenthal, Y., Bassinot, F., and Beaufort, L.: Stable sea surface temperatures in the western Pacific warm pool over the past 1.75 million years, Nature, 433, 294–298, https://doi.org/10.1038/nature03189, 2005.

De La Vega, E., Chalk, T. B., Wilson, P. A., Bysani, R. P., and Foster, G. L.: Atmospheric CO2 during the Mid-Piacenzian Warm Period and the M2 glaciation, Scientific Reports, 10, 11 002, https://doi.org/10.1038/s41598-020-67154-8, 2020.

Delworth, T. L., Zeng, F., Vecchi, G. A., Yang, X., Zhang, L., and Zhang, R.: The North Atlantic Oscillation as a driver of rapid climate change in the Northern Hemisphere, Nature Geoscience, 9, 509–512, https://doi.org/10.1038/ngeo2738, 2016.

Diamond, R., Sime, L. C., Schroeder, D., Jackson, L. C., Holland, P. R., De Asenjo, E. A., Bellomo, K., Danabasoglu, G., Hu, A., Jungclaus, J., Montoya, M., Meccia, V. L., Saenko, O. A., and Swingedouw, D.: A Weakened AMOC Could Cause Southern Ocean Temperature and Sea-Ice Change on Multidecadal Timescales, Journal of Geophysical Research: Oceans, 130, e2024JC022 027, https://doi.org/10.1029/2024JC022027, 2025.

Dowsett, H., Dolan, A., Rowley, D., Moucha, R., Forte, A. M., Mitrovica, J. X., Pound, M., Salzmann, U., Robinson, M., Chandler, M., Foley, K., and Haywood, A.: The PRISM4 (mid-Piacenzian) paleoenvironmental reconstruction, Climate of the Past, 12, 1519–1538, https://doi.org/10.5194/cp-12-1519-2016, 2016.

Dyez, K. A. and Ravelo, A. C.: Late Pleistocene tropical Pacific temperature sensitivity to radiative greenhouse gas forcing, Geology, 41, 23–26, https://doi.org/10.1130/G33425.1, 2013.

Dyez, K. A., Hönisch, B., and Schmidt, G. A.: Early Pleistocene Obliquity-Scale pCO_2 Variability at ~1.5 Million Years Ago, Paleoceanography and Paleoclimatology, 33, 1270–1291, https://doi.org/10.1029/2018PA003349, 2018.

Essery, R., Best, M., and Cox, P.: MOSES 2.2 technical documentation, 2001.

Farmer, J. R., Hönisch, B., Haynes, L. L., Kroon, D., Jung, S., Ford, H. L., Raymo, M. E., Jaume-Seguí, M., Bell, D. B., Goldstein, S. L., Pena, L. D., Yehudai, M., and Kim, J.: Deep Atlantic Ocean carbon storage and the rise of 100,000-year glacial cycles, Nature Geoscience, 12, 355–360, https://doi.org/10.1038/s41561-019-0334-6, 2019.

Ferrari, R., Jansen, M. F., Adkins, J. F., Burke, A., Stewart, A. L., and Thompson, A. F.: Antarctic sea ice control on ocean circulation in present and glacial climates, Proceedings of the National Academy of Sciences, 111, 8753–8758, https://doi.org/10.1073/pnas.1323922111, 2014.

Ford, H. L. and Ravelo, A. C.: Estimates of Pliocene Tropical Pacific Temperature Sensitivity to Radiative Greenhouse Gas Forcing, Paleoceanography and Paleoclimatology, 34, 2–15, https://doi.org/10.1029/2018PA003461, 2019.

Ganopolski, A. and Calov, R.: The role of orbital forcing, carbon dioxide and regolith in 100 kyr glacial cycles, Climate of the Past, 7, 1415–1425, https://doi.org/10.5194/cp-7-1415-2011, 2011.

https://doi.org/10.5194/egusphere-2026-3719
Preprint. Discussion started: 8 July 2026

Gordon, C., Gregory, J. M., and Wood, R. A.: The simulation of SST, sea ice extents and ocean heat transports in a version of the Hadley Centre coupled model without ¯ux adjustments, 2000.

Hasenfratz, A. P., Jaccard, S. L., Martínez-García, A., Sigman, D. M., Hodell, D. A., Vance, D., Bernasconi, S. M., Kleiven, H. K. F., Haumann, F. A., and Haug, G. H.: The residence time of Southern Ocean surface waters and the 100,000-year ice age cycle, Science, 363, 1080–1084, https://doi.org/10.1126/science.aat7067, 2019.

Haywood, A., Tindall, J., Burton, L., Chandler, M., Dolan, A., Dowsett, H., Feng, R., Fletcher, T., Foley, K., Hill, D., Hunter, S., Otto-Bliesner, B., Lunt, D., Robinson, M., and Salzmann, U.: Pliocene Model Intercomparison Project Phase 3 (PlioMIP3) – Science plan and experimental design, Global and Planetary Change, 232, 104 316, https://doi.org/10.1016/j.gloplacha.2023.104316, 2024.

Haywood, A. M., Dowsett, H. J., Dolan, A. M., Rowley, D., Abe-Ouchi, A., Otto-Bliesner, B., Chandler, M. A., Hunter, S. J., Lunt, D. J., Pound, M., and Salzmann, U.: The Pliocene Model Intercomparison Project (PlioMIP) Phase 2: scientific objectives and experimental design, Climate of the Past, 12, 663–675, https://doi.org/10.5194/cp-12-663-2016, 2016.

Haywood, A. M., Tindall, J. C., Dowsett, H. J., Dolan, A. M., Foley, K. M., Hunter, S. J., Hill, D. J., Chan, W.-L., Abe-Ouchi, A., Stepanek, C., Lohmann, G., Chandan, D., Peltier, W. R., Tan, N., Contoux, C., Ramstein, G., Li, X., Zhang, Z., Guo, C., Nisancioglu, K. H., Zhang, Q., Li, Q., Kamae, Y., Chandler, M. A., Sohl, L. E., Otto-Bliesner, B. L., Feng, R., Brady, E. C., Von Der Heydt, A. S., Baatsen, M. L. J., and Lunt, D. J.: The Pliocene Model Intercomparison Project Phase 2: large-scale climate features and climate sensitivity, Climate of the Past, 16, 2095–2123, https://doi.org/10.5194/cp-16-2095-2020, 2020.

Herbert, T. D.: The Mid-Pleistocene Climate Transition, Annual Review of Earth and Planetary Sciences, 51, 389–418, https://doi.org/10.1146/annurev-earth-032320-104209, 2023.

Hines, S. K. V., Charles, C. D., Starr, A., Goldstein, S. L., Hemming, S. R., Hall, I. R., Lathika, N., Passacantando, M., and Bolge, L.: Revisiting the mid-Pleistocene transition ocean circulation crisis, Science, 386, 681–686, https://doi.org/10.1126/science.adn4154, 2024.

Hopcroft, P. O. and Valdes, P. J.: Paleoclimate-conditioning reveals a North Africa land–atmosphere tipping point, Proceedings of the National Academy of Sciences, 118, e2108783 118, https://doi.org/10.1073/pnas.2108783118, 2021.

Hopcroft, P. O., Valdes, P. J., and Ingram, W.: Using the mid-Holocene 'greening' of the Sahara to narrow acceptable ranges on climate model parameters, https://doi.org/10.1002/essoar.10505398.1, 2020.

Izumi, K., Valdes, P., Ivanovic, R., and Gregoire, L.: Impacts of the PMIP4 ice sheets on Northern Hemisphere climate during the last glacial period, Climate Dynamics, 60, 2481–2499, https://doi.org/10.1007/s00382-022-06456-1, 2023.

Kageyama, M., Harrison, S. P., Kapsch, M.-L., Lofverstrom, M., Lora, J. M., Mikolajewicz, U., Sherriff-Tadano, S., Vadsaria, T., Abe-Ouchi, A., Bouttes, N., Chandan, D., Gregoire, L. J., Ivanovic, R. F., Izumi, K., LeGrande, A. N., Lhardy, F., Lohmann, G., Morozova, P. A., Ohgaito, R., Paul, A., Peltier, W. R., Poulsen, C. J., Quiquet, A., Roche, D. M., Shi, X., Tierney, J. E., Valdes, P. J., Volodin, E., and Zhu, J.: The PMIP4 Last Glacial Maximum experiments: preliminary results and comparison with the PMIP3 simulations, Climate of the Past, 17, 1065–1089, https://doi.org/10.5194/cp-17-1065-2021, 2021.

Khider, D., Emile-Geay, J., Zhu, F., James, A., Landers, J., Ratnakar, V., and Gil, Y.: Pyleoclim: Paleoclimate Timeseries Analysis and Visualization With Python, Paleoceanography and Paleoclimatology, 37, e2022PA004 509, https://doi.org/10.1029/2022PA004509, 2022.

Kleiven, H. F., Jansen, E., Fronval, T., and Smith, T. M.: Intensi¢cation of Northern Hemisphere glaciations in the circum Atlantic region (3.5^2.4 Ma) ^ ice-rafted detritus evidence, 2002.

Köhler, P.: Atmospheric CO_2 Concentration Based on Boron Isotopes Versus Simulations of the Global Carbon Cycle During the Plio-Pleistocene, Paleoceanography and Paleoclimatology, 38, e2022PA004 439, https://doi.org/10.1029/2022PA004439, 2023.

https://doi.org/10.5194/egusphere-2026-3719
Preprint. Discussion started: 8 July 2026

Laskar, J., Robutel, P., Joutel, F., Gastineau, M., Correia, A. C. M., and Levrard, B.: A long-term numerical solution for the insolation quantities of the Earth, Astronomy & Astrophysics, 428, 261–285, https://doi.org/10.1051/0004-6361:20041335, 2004.

Liu, W. and Fedorov, A.: Interaction between Arctic sea ice and the Atlantic meridional overturning circulation in a warming climate, Climate Dynamics, 58, 1811–1827, https://doi.org/10.1007/s00382-021-05993-5, 2022.

Lo, L., Belt, S. T., Lattaud, J., Friedrich, T., Zeeden, C., Schouten, S., Smik, L., Timmermann, A., Cabedo-Sanz, P., Huang, J.-J., Zhou, L., Ou, T.-H., Chang, Y.-P., Wang, L.-C., Chou, Y.-M., Shen, C.-C., Chen, M.-T., Wei, K.-Y., Song, S.-R., Fang, T.-H., Gorbarenko, S. A., Wang, W.-L., Lee, T.-Q., Elderfield, H., and Hodell, D. A.: Precession and atmospheric CO2 modulated variability of sea ice in the central Okhotsk Sea since 130,000 years ago, Earth and Planetary Science Letters, 488, 36–45, https://doi.org/10.1016/j.epsl.2018.02.005, 2018.

Loulergue, L., Schilt, A., Spahni, R., Masson-Delmotte, V., Blunier, T., Lemieux, B., Barnola, J.-M., Raynaud, D., Stocker, T. F., and Chappellaz, J.: Orbital and millennial-scale features of atmospheric CH4 over the past 800,000 years, Nature, 453, 383–386, https://doi.org/10.1038/nature06950, 2008.

Lunt, D. J., Williamson, M. S., Valdes, P. J., Lenton, T. M., and Marsh, R.: Comparing transient, accelerated, and equilibrium simulations of the last 30 000 years with the GENIE-1 model, Clim. Past, 2006.

Marks-Peterson, J., Shackleton, S., Higgins, J., Severinghaus, J., Yan, Y., Buizert, C., Kalk, M., Beaudette, R., Hishamunda, V., Eves, D., Carter, A., Kurbatov, A., Epifanio, J., Morgan, J., Nesbitt, I., Bender, M., and Brook, E.: Broadly stable atmospheric CO2 and CH4 levels over the past 3 million years, Nature, 651, 647–652, https://doi.org/10.1038/s41586-025-10032-y, 2026.

Martínez-Garcia, A., Rosell-Melé, A., Jaccard, S. L., Geibert, W., Sigman, D. M., and Haug, G. H.: Southern Ocean dust–climate coupling over the past four million years, Nature, 476, 312–315, https://doi.org/10.1038/nature10310, 2011.

Marzocchi, A. and Jansen, M. F.: Global cooling linked to increased glacial carbon storage via changes in Antarctic sea ice, Nature Geoscience, 12, 1001–1005, https://doi.org/10.1038/s41561-019-0466-8, 2019.

McClymont, E. L., Ford, H. L., Ho, S. L., Tindall, J. C., Haywood, A. M., Alonso-Garcia, M., Bailey, I., Berke, M. A., Littler, K., Patterson, M. O., Petrick, B., Peterse, F., Ravelo, A. C., Risebrobakken, B., De Schepper, S., Swann, G. E. A., Thirumalai, K., Tierney, J. E., Van Der Weijst, C., White, S., Abe-Ouchi, A., Baatsen, M. L. J., Brady, E. C., Chan, W.-L., Chandan, D., Feng, R., Guo, C., Von Der Heydt, A. S., Hunter, S., Li, X., Lohmann, G., Nisancioglu, K. H., Otto-Bliesner, B. L., Peltier, W. R., Stepanek, C., and Zhang, Z.: Lessons from a high-CO_2 world: an ocean view from $\sim$ 3 million years ago, Climate of the Past, 16, 1599–1615, https://doi.org/10.5194/cp-16-1599-2020, 2020.

Menviel, L.: The southern amplifier, Science, 363, 1040–1041, https://doi.org/10.1126/science.aaw7196, 2019.

Panieri, G., Knies, J., Vadakkepuliyambatta, S., Lee, A. L., and Schubert, C. J.: Evidence of Arctic methane emissions across the mid-Pleistocene, Communications Earth & Environment, 4, 109, https://doi.org/10.1038/s43247-023-00772-y, 2023.

Pena, L. D. and Goldstein, S. L.: Thermohaline circulation crisis and impacts during the mid-Pleistocene transition, Science, 345, 318–322, https://doi.org/10.1126/science.1249770, 2014.

Pisias, N. and Moore, T.: The evolution of Pleistocene climate: A time series approach, Earth and Planetary Science Letters, 52, 450–458, https://doi.org/10.1016/0012-821X(81)90197-7, 1981.

Pope, V. D., Gallani, M. L., Rowntree, P. R., and Stratton, R. A.: The impact of new physical parametrizations in the Hadley Centre climate model: HadAM3, Climate Dynamics, 16, 123–146, https://doi.org/10.1007/s003820050009, 2000.

Raymo, M. E.: The timing of major climate terminations, Paleoceanography, 12, 577–585, https://doi.org/10.1029/97PA01169, 1997.

Raymo, M. E. and Nisancioglu, K. H.: The 41 kyr world: Milankovitch's other unsolved mystery, Paleoceanography, 18, https://doi.org/10.1029/2002pa000791, 2003.

https://doi.org/10.5194/egusphere-2026-3719
Preprint. Discussion started: 8 July 2026

Rohling, E. J., Foster, G. L., Grant, K. M., Marino, G., Roberts, A. P., Tamisiea, M. E., and Williams, F.: Sea-level and deep-sea-temperature variability over the past 5.3 million years, Nature, 508, 477–482, https://doi.org/10.1038/nature13230, 2014.

Shackleton, N. J. and Opdyke, N. D.: Oxygen isotope and palaeomagnetic evidence for early Northern Hemisphere glaciation, Nature, 270, 216–219, https://doi.org/10.1038/270216a0, 1977.

Shakun, J. D.: Modest global-scale cooling despite extensive early Pleistocene ice sheets, Quaternary Science Reviews, 165, 25–30, https://doi.org/10.1016/j.quascirev.2017.04.010, 2017.

Shin, S., Liu, Z., Otto-Bliesner, B. L., Kutzbach, J. E., and Vavrus, S. J.: Southern Ocean sea-ice control of the glacial North Atlantic thermohaline circulation, Geophysical Research Letters, 30, 2002GL015 513, https://doi.org/10.1029/2002GL015513, 2003.

Singarayer, J. and Valdes, P. J.: High-latitude climate sensitivity to ice-sheet forcing over the last 120kyr, Quaternary Science Reviews, 29, 43–55, https://doi.org/10.1016/j.quascirev.2009.10.011, 2010.

Sosdian, S. and Rosenthal, Y.: Deep-Sea Temperature and Ice Volume Changes Across the Pliocene-Pleistocene Climate Transitions, Science, 325, 306–310, https://doi.org/10.1126/science.1169938, 2009.

Spahni, R., Chappellaz, J., Stocker, T. F., Loulergue, L., Hausammann, G., Kawamura, K., Flückiger, J., Schwander, J., Raynaud, D., Masson-Delmotte, V., and Jouzel, J.: Atmospheric Methane and Nitrous Oxide of the Late Pleistocene from Antarctic Ice Cores, Science, 310, 1317–1321, https://doi.org/10.1126/science.1120132, 2005.

Stap, L. B., Köhler, P., and Lohmann, G.: Including the efficacy of land ice changes in deriving climate sensitivity from paleodata, Earth System Dynamics, 10, 333–345, https://doi.org/10.5194/esd-10-333-2019, 2019.

Steinig, S., Abe-Ouchi, A., De Boer, A. M., Chan, W.-L., Donnadieu, Y., Hutchinson, D. K., Knorr, G., Ladant, J.-B., Morozova, P., Niezgodzki, I., Poulsen, C. J., Volodin, E. M., Zhang, Z., Zhu, J., Evans, D., Inglis, G. N., Meckler, A. N., and Lunt, D. J.: DeepMIP-Eocene-p1: multi-model dataset and interactive web application for Eocene climate research, Scientific Data, 11, 970, https://doi.org/10.1038/s41597-024-03773-4, 2024.

Timm, O. and Timmermann, A.: Simulation of the Last 21 000 Years Using Accelerated Transient Boundary Conditions*, Journal of Climate, 20, 4377–4401, https://doi.org/10.1175/JCLI4237.1, 2007.

Timmermann, A., Friedrich, T., Timm, O. E., Chikamoto, M. O., Abe-Ouchi, A., and Ganopolski, A.: Modeling Obliquity and CO2 Effects on Southern Hemisphere Climate during the Past 408 ka, 2014.

Torrence, C. and Compo, G. P.: A Practical Guide to Wavelet Analysis, Bulletin of the American Meteorological Society, 79, 61–78, https://doi.org/10.1175/1520-0477(1998)079<0061:APGTWA>2.0.CO;2, 1998.

Tzedakis, P. C., Crucifix, M., Mitsui, T., and Wolff, E. W.: A simple rule to determine which insolation cycles lead to interglacials, Nature, 542, 427–432, https://doi.org/10.1038/nature21364, 2017.

Valdes, Armstrong, E., Badger, M. P. S., Bradshaw, C. D., Bragg, F., Crucifix, M., Davies-Barnard, T., Day, J. J., Farnsworth, A., Gordon, C., Hopcroft, P. O., Kennedy, A. T., Lord, N. S., Lunt, D. J., Marzocchi, A., Parry, L. M., Pope, V., Roberts, W. H. G., Stone, E. J., Tourte, G. J. L., and Williams, J. H. T.: The BRIDGE HadCM3 family of climate models: HadCM3@Bristol v1.0, Geoscientific Model Development, 10, 3715–3743, https://doi.org/10.5194/gmd-10-3715-2017, 2017.

Varma, V., Prange, M., and Schulz, M.: Transient simulations of the present and the last interglacial climate using the Community Climate System Model version 3: effects of orbital acceleration, Geoscientific Model Development, 9, 3859–3873, https://doi.org/10.5194/gmd-9-3859-2016, 2016.

Westerhold, T., Marwan, N., Drury, A. J., Liebrand, D., Agnini, C., Anagnostou, E., Barnet, J. S. K., Bohaty, S. M., De Vleeschouwer, D., Florindo, F., Frederichs, T., Hodell, D. A., Holbourn, A. E., Kroon, D., Lauretano, V., Littler, K., Lourens, L. J., Lyle, M., Pälike, H., Röhl,

https://doi.org/10.5194/egusphere-2026-3719
Preprint. Discussion started: 8 July 2026

U., Tian, J., Wilkens, R. H., Wilson, P. A., and Zachos, J. C.: An astronomically dated record of Earth's climate and its predictability over the last 66 million years, Science, 369, 1383–1387, https://doi.org/10.1126/science.aba6853, 2020.

Willeit, M., Ganopolski, A., Calov, R., and Brovkin, V.: Mid-Pleistocene transition in glacial cycles explained by declining CO2 and regolith removal, SCIENCE ADVANCES, 2019.

Wu, Z., Yin, Q., Guo, Z., and Berger, A.: Hemisphere differences in response of sea surface temperature and sea ice to precession and obliquity, Global and Planetary Change, 192, 103 223, https://doi.org/10.1016/j.gloplacha.2020.103223, 2020.

Yan, Y., Bender, M. L., Brook, E. J., Clifford, H. M., Kemeny, P. C., Kurbatov, A. V., Mackay, S., Mayewski, P. A., Ng, J., Severinghaus, J. P., and Higgins, J. A.: Two-million-year-old snapshots of atmospheric gases from Antarctic ice, Nature, 574, 663–666, https://doi.org/10.1038/s41586-019-1692-3, 2019.

Yun, K.-S., Timmermann, A., Lee, S.-S., Willeit, M., Ganopolski, A., and Jadhav, J.: A transient coupled general circulation model (CGCM) simulation of the past 3 million years, Climate of the Past, 19, 1951–1974, https://doi.org/10.5194/cp-19-1951-2023, 2023.

Zelinka, M. D., Myers, T. A., McCoy, D. T., Po-Chedley, S., Caldwell, P. M., Ceppi, P., Klein, S. A., and Taylor, K. E.: Causes of Higher Climate Sensitivity in CMIP6 Models, Geophysical Research Letters, 47, e2019GL085 782, https://doi.org/10.1029/2019GL085782, 2020.

Zeller, E., Timmermann, A., Yun, K.-S., Raia, P., Stein, K., and Ruan, J.: Human adaptation to diverse biomes over the past 3 million years, Science, 380, 604–608, https://doi.org/10.1126/science.abq1288, 2023.